The MODIS Aerosol Algorithm, Products, and Validation

L. A. REMER,* Y. J. KAUFMAN,* D. TANRÉ,+ S. MATTOO,*,& D. A. CHU,#,** J. V. MARTINS,*,++ R.-R. LI,#,## C. ICHOKU,*,& R. C. LEVY,*,& R. G. KLEIDMAN,*,& T. F. ECK,@,@@ E. VERMOTE,@,&& AND B. N. HOLBEN@

*Laboratory for Atmospheres, NASA Goddard Space Flight Center, Greenbelt, Maryland
+Laboratoire d'Optique Atmospherique, Université des Sciences et Technologies de Lille, Villenueve d'Ascq, France
#Laboratory for Atmospheres, NASA Goddard Space Flight Center, Greenbelt, Maryland
@Laboratory for Terrestrial Physics, NASA Goddard Space Flight Center, Greenbelt, Maryland

(Manuscript received 15 August 2003, in final form 8 June 2004)

ABSTRACT

The Moderate Resolution Imaging Spectroradiometer (MODIS) aboard both NASA's *Terra* and *Aqua* satellites is making near-global daily observations of the earth in a wide spectral range (0.41–15 μm). These measurements are used to derive spectral aerosol optical thickness and aerosol size parameters over both land and ocean. The aerosol products available over land include aerosol optical thickness at three visible wavelengths, a measure of the fraction of aerosol optical thickness attributed to the fine mode, and several derived parameters including reflected spectral solar flux at the top of the atmosphere. Over the ocean, the aerosol optical thickness is provided in seven wavelengths from 0.47 to 2.13 μm. In addition, quantitative aerosol size information includes effective radius of the aerosol and quantitative fraction of optical thickness attributed to the fine mode. Spectral irradiance contributed by the aerosol, mass concentration, and number of cloud condensation nuclei round out the list of available aerosol products over the ocean. The spectral optical thickness and effective radius of the aerosol over the ocean are validated by comparison with two years of Aerosol Robotic Network (AERONET) data gleaned from 132 AERONET stations. Eight thousand MODIS aerosol retrievals collocated with AERONET measurements confirm that one standard deviation of MODIS optical thickness retrievals fall within the predicted uncertainty of $\Delta\tau = \pm 0.03 \pm 0.05\tau$ over ocean and $\Delta\tau = \pm 0.05 \pm 0.15\tau$ over land. Two hundred and seventy-one MODIS aerosol retrievals collocated with AERONET inversions at island and coastal sites suggest that one standard deviation of MODIS effective radius retrievals falls within $\Delta r_{\mathrm{eff}} = \pm 0.11$ μm. The accuracy of the MODIS retrievals suggests that the product can be used to help narrow the uncertainties associated with aerosol radiative forcing of global climate.

& Additional affiliation: Science Systems and Applications, Inc., Lanham, Maryland.
** Current affiliation: Joint Center for Earth Systems Technology, University of Maryland, Baltimore County, Baltimore, Maryland.
++ Additional affiliation: Joint Center for Earth Systems Technology, University of Maryland, Baltimore County, Baltimore, Maryland.
Current affiliation: Goddard Earth Sciences and Technology Center, University of Maryland, Baltimore County, Baltimore, Maryland.
@@ Additional affiliation: Goddard Earth Sciences and Technology Center, University of Maryland, Baltimore County, Baltimore, Maryland.
&& Additional affiliation: Department of Geography, University of Maryland, College Park, College Park, Maryland.

Corresponding author address: Dr. Lorraine Remer, Code 913, NASA Goddard Space Flight Center, Greenbelt, MD 20771.
E-mail: Lorraine.A.Remer@nasa.gov

© 2005 American Meteorological Society

1. Introduction

The Chesapeake Lighthouse and Aircraft Measurements for Satellites (CLAMS) field experiment was designed to aid the development and evaluation of satellite algorithms that retrieve geophysical parameters important to the earth's radiative balance and estimates of global change. Aerosols are one of those important geophysical parameters that determine the earth's energy balance and hydrological cycle. These suspended airborne particles scatter solar radiation back, absorb solar radiation in the atmosphere, and shade the earth's surface. Airborne particles act as cloud condensation nuclei entering into cloud processes and thereby change cloud reflectivity and the hydrological cycle (Twomey 1977; Rosenfield and Lensky 1998). Aerosols also affect human health and reduce visibility (Samet et al. 2000). Some aerosol types are natural, such as wind-blown desert dust or sea salt caused by breaking waves. Other aerosol types are created from human activities such as urban/industrial pollution and biomass burning. Unlike CO_2, another atmospheric pollutant input into the atmosphere from human activity, aerosols are not well mixed in the atmosphere and, because of their spatial and temporal variability, the uncertainty of estimating human-induced aerosol forcing on climate and the hydrological cycle is on the order of 2 W m^{-2}, which is equal to the estimated forcing of all the greenhouse gases combined (Houghton et al. 2001). Therefore, characterizing global aerosol distribution presents one of our major challenges today (Kaufman et al. 2002).

Operational remote sensing of aerosols from long-term satellites provides a means to achieve a global and seasonal characterization of aerosol. Satellite sensors view the entire earth and produce global images, thus resolving the spatial patterns resulting from the spatial inhomogeneities of aerosol sources. Daily global images from polar-orbiting satellites (Husar et al. 1997; Herman et al. 1997; Torres et al. 2002) and more frequent imagery from geostationary satellites (Prins et al. 1998) resolve the temporal patterns resulting from the short lifetimes of aerosols, which are on the order of a few days to a week.

The Moderate Resolution Imaging Spectroradiometer (MODIS) is a new sensor with the ability to characterize the spatial and temporal characteristics of the global aerosol field. Launched aboard NASA's *Terra* and *Aqua* satellites in December 1999 and May 2002, MODIS has 36 channels spanning the spectral range from 0.41 to 15 μm representing three spatial resolutions: 250 m (2 channels), 500 m (5 channels), and 1 km (29 channels). The aerosol retrieval makes use of seven of these channels (0.47–2.13 μm) to retrieve aerosol characteristics and uses additional wavelengths in other parts of the spectrum to identify clouds and river sediments (Ackerman et al. 1998; Gao et al. 2002; Martins et al. 2002; Li et al. 2003). Unlike previous satellite sensors, which did not have sufficient spectral diversity, MODIS has the unique ability to retrieve aerosol optical thickness with greater accuracy and to retrieve parameters characterizing aerosol size (Tanré et al. 1996; Tanré et al. 1997). The results section of this paper shows that MODIS's ability to separate aerosols by size can be used as a proxy for separating human-generated aerosol from natural sources, which aids substantially in estimating global human-induced aerosol forcing (Kaufman et al. 2002).

The first MODIS instrument was launched aboard *Terra* at the end of 1999 and began transmitting data at the end of February 2000. Algorithms were in place, designed to use the observed radiances to derive many important aerosol products. Early comparisons of the retrieved aerosol parameters with ground-based validation data showed remarkable agreement between the two types of data (Chu et al. 2002; Remer et al. 2002), but also showed us situations in which the algorithms could be improved. Almost immediately, the algorithms were modified to reflect a better understanding of the instrument's capabilities and the nature of aerosols and clouds. In a companion study in this special issue, the MODIS aerosol algorithm over ocean is compared with an independent aerosol retrieval algorithm applied to the same dataset of MODIS radiances (Ignatov et al. 2005). In another companion paper in this special issue, the MODIS retrievals over land and ocean are evaluated regionally for the specific time and location of the CLAMS field study using the additional resources available during the CLAMS intensive observing period (Levy et al. 2005). However, in the present study we take a global view. We give a comprehensive description of the MODIS aerosol algorithms, highlighting the changes that were implemented postlaunch. We describe the wealth of aerosol products derived from MODIS data and available to any user. Last, we show some of the global comparisons to ground-based data as validation for the products previously described.

2. MODIS aerosol algorithms

The MODIS aerosol algorithm is actually two entirely independent algorithms, one for deriving aerosols over land and the second for aerosols over ocean. Both algorithms were conceived and developed before the *Terra* launch and are described in depth in Kaufman et al. (1997a) and Tanré et al. (1997). In addition, Levy et al. (2003) provide a more recent description of the over-ocean retrieval algorithm. Both the land and ocean aerosol algorithms rely on calibrated, geolocated reflectances provided by the MODIS Characterization Support Team (MCST), identified as products MOD02 and MOD03 for *Terra* MODIS products and MYD02 and MYD03 for the *Aqua* MODIS products (MCST 2000, 2002). The uncertainties in these measured reflectances in the visible and mid-IR bands are less than 2% (Guenther et al. 2002). Ignatov et al. (2005) provides a

good discussion of these reflectances and possible errors associated with them. These reflectances along with the MODIS cloud mask product identified as MOD/MYD35 (Ackerman et al. 1998) and meteorological data from the National Centers for Environmental Prediction (NCEP) provide the input for the algorithms. The MOD/MYD35 cloud mask product also supplies the earth's surface information that identifies whether a pixel is a "land" pixel or a "water" pixel. Although the algorithm inputs the NCEP data, it can run successfully without these supplements by using climatology for first-guess water vapor and ozone profiles.

The theoretical basis of the algorithms has not changed from inception, although some of the mechanics and details of the algorithms have evolved. MODIS data are organized by "Collections." A collection consists of data products that were generated by similar, but not necessarily the same, versions of the algorithm. (A complete history of changes to the algorithm over the course of the MODIS mission can be found online at http://modis-atmos.gsfc.nasa.gov/MOD04_L2/history.html.) In this section we leave the explanation of the theoretical basis of the algorithms to the earlier references and, instead, focus on the mechanics of the V4.2.2 algorithm presently in operation, highlighting the changes made since 1997.

The data analysis that follows uses data from the MODIS sensor aboard the *Terra* satellite from both *Terra* Collections 003 and 004, generated by various versions of the algorithm beginning with V3.1.0; V4.2.2 will be used to reprocess all previous data to Collection 004, and then eventually to Collection 005. However, a complete 2-yr dataset of Collection 004 data was not available at the time of the analysis for this paper. Although there are subtle differences in the two collections, the essential characters of the derived products in *Terra* Collections 003 and 004 remain the same, and thus are combined for the analyses in the sections that follow. A comprehensive comparison of the primary products of the two *Terra* collections and one *Aqua* collection can be found in Ichoku et al. (2005).

a. The land algorithm

Figure 1 illustrates the mechanics of the land algorithm. An individual MODIS image scene, called a granule, consists of a 5-min swath of data. The MODIS level 1b granule consists of calibrated radiances or reflectances. These reflectances are corrected for water vapor, ozone, and carbon dioxide before the algorithm proceeds. The first step in deriving aerosol products over land is to organize the measured reflectances of the three MODIS channels used in the procedure: $\rho_{0.47}$, $\rho_{0.66}$, and $\rho_{2.13}$. All three channels are organized into nominal 10-km boxes corresponding to 20 by 20, or 400 pixels for each box. This organization requires the 250-m resolution 0.66-μm channel to be degraded to 500 m in order to match the resolution of the other two channels.

1) SELECTION OF PIXELS

The 400 pixels in the box are evaluated pixel by pixel to identify whether the pixel is cloudy, snow/ice, or water. The land algorithm will retrieve aerosol for coastal boxes that contain one or more pixels identified as ocean, but will decrease the quality of that land retrieval. An ocean retrieval requires all 400 pixels in the box to be identified as water. Originally, the standard MODIS cloud mask (MOD/MYD35) provided all masking information. Since launch, additional masking has been put in place, including most recently an internal cloud mask based on spatial variability to identify low clouds and the reflectance in the 1.38-μm channel to identify high clouds. Because the algorithm is sensitive to small subpixel patches of snow/ice, now all eight pixels contiguous to a pixel identified as "snow/ice" by MOD35 will also be labeled as "snow/ice." The pixels are further screened for subpixel water by determining the value of the Normalized Difference Vegetation Index (NDVI) for each pixel. Values of NDVI less than 0.10 are identified as containing subpixel water and are excluded along with cloudy and snowy pixels from the remainder of the algorithm.

2) DETERMINATION OF SURFACE REFLECTANCE

This process is described in Kaufman et al. (1997a), with the following modifications: The algorithm now includes brighter surfaces, which expands the geographical extent of the land retrieval. The reflectance at 3.8 μm is no longer considered, and dark pixels are selected based only on their reflectance at 2.13 μm. To be selected, a pixel must fall within the range of $0.01 \leq \rho_{2.13} \leq 0.25$. Experimentation with the operational retrieval showed us that $\rho_{2.13}$ values as bright as 0.25 gave us the same accuracy as the more conservative value of 0.15 initially proposed in Kaufman et al. (1997a). The pixels remaining after masking and dark target selection are then sorted in terms of their visible reflectance, $\rho_{0.66}$. The pixels with the darkest 20% and brightest 50% of $\rho_{0.66}$ are discarded. The reason is to eliminate remaining pixels possibly contaminated by cloud shadows or odd surfaces at the dark end or residual cloud contamination and odd surfaces at the bright end. The possibility of residual bright cloud contamination is more common than cloud shadows; thus the filter is skewed toward permitting more dark pixels than bright ones. The remaining 30% of the pixels will be the ones used in the regular retrieval path, labeled path A in Fig. 1, but only if there are at least 12 of these pixels remaining from the original 400 in the 20 × 20 box. The mean measured reflectance is calculated from these 12 or more dark target pixels in the three wavelengths ($\overline{\rho}_{0.47}$, $\overline{\rho}_{0.66}$, and $\overline{\rho}_{2.13}$). The surface reflectances at 0.47 and 0.66 μm ($\rho^{s}_{0.47}$, $\rho^{s}_{0.66}$) are derived from the mean measured $\overline{\rho}_{2.13}$ value using the empirical relationships,

$$\rho^{s}_{0.47} = 0.25\,\rho_{2.13};\ \rho^{s}_{0.66} = 0.50\,\rho_{2.13}, \qquad (1)$$

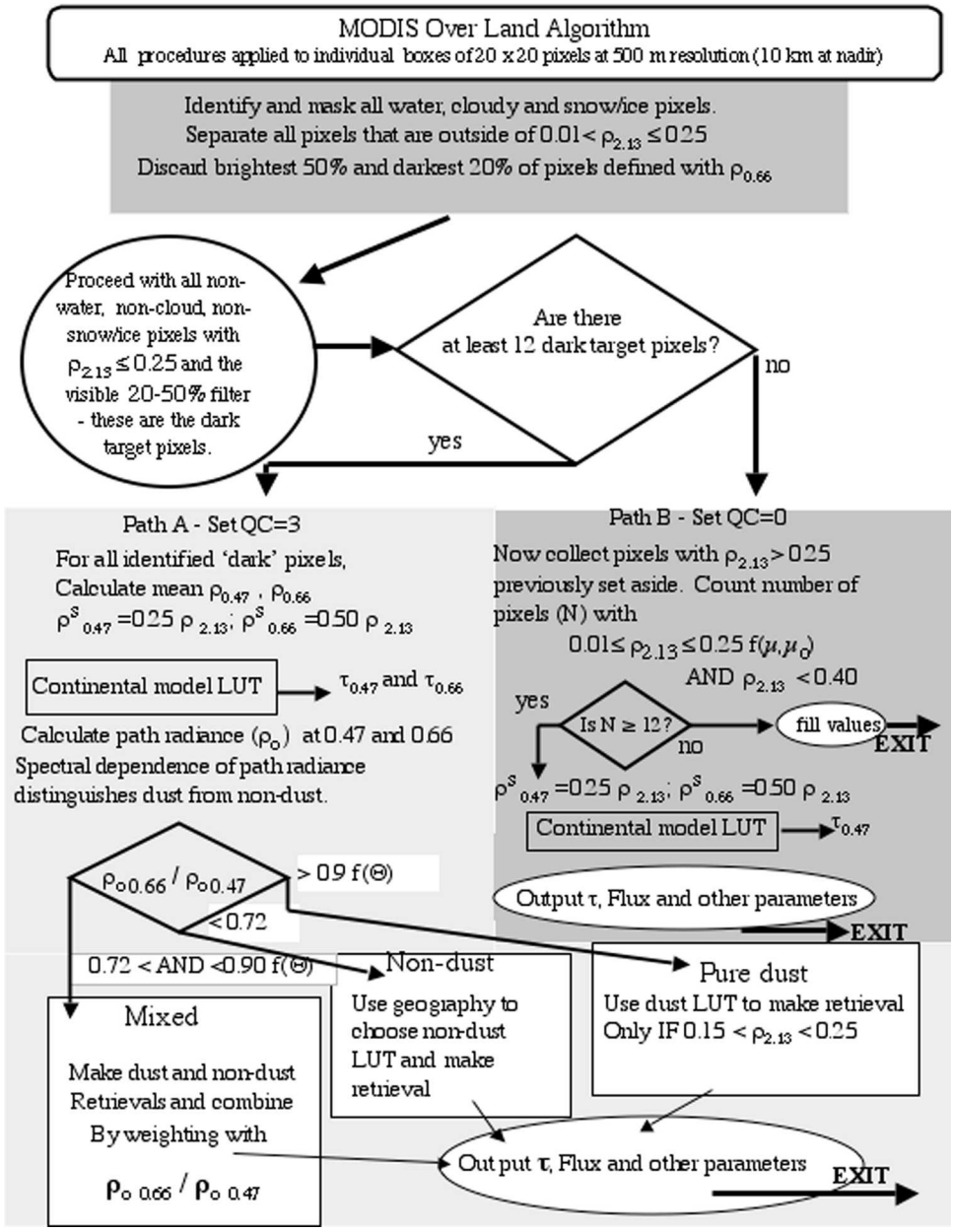

FIG. 1. Flowchart illustrating the derivation of aerosol over land.

as described in Kaufman et al. (1997a,b). A retrieval following path A is given a quality control value of 3, "very good." An alternative path used for brighter surfaces is described below.

3) CHOOSING THE AEROSOL MODELS

The estimated surface reflectances ($\rho^s_{0.47}$, $\rho^s_{0.66}$) and the measured mean top-of-atmosphere reflectances ($\overline{\rho}_{0.47}$, $\overline{\rho}_{0.66}$) are used as input into the continental model lookup table (LUT) to retrieve values for the aerosol optical thickness at 0.47 and 0.66 μm ($\tau_{0.47}$, $\tau_{0.66}$). In the land algorithm, the two wavelengths are derived independently. The retrieved optical thicknesses along with the continental model's single scattering albedoes ($\omega_{o0.47}$, $\omega_{o0.66}$) and phase functions ($P_{0.47}$, $P_{0.66}$) at the appropriate scattering angle are used to calculate the path radiance in each wavelength using the single scattering approximation:

$$\rho_{o0.47} = \omega_{o0.47}\tau_{0.47}P_{0.47};$$
$$\rho_{o0.66} = \omega_{o0.66}\tau_{0.66}P_{0.66}, \quad (2)$$

where $\rho_{o0.47}$ and $\rho_{o0.66}$ are the path radiances at 0.47 and 0.66 μm, respectively. The spectral dependence of the path radiance distinguishes between dust (dominated

by coarse mode) and nondust (dominated by fine mode). Kaufman et al. (1997a) describes how the algorithm uses the ratio of path radiances, $\rho_{o0.66}/\rho_{o0.47}$, to make a three-branched decision whether the aerosol is pure dust, nondust, or mixed. Using the continental model does not impact the resulting ratio. It is simply used to remove the molecular and surface contributions and to isolate the aerosol reflectance in both channels. The thresholds for the decision tree are

$$\rho_{o0.66}/\rho_{o\,0.47} < 0.72 \text{ THEN pure nondust} \tag{3a}$$

$$\rho_{o0.66}/\rho_{o0.47} > 0.9 - 0.01(\Theta - 150°) \text{ THEN pure dust} \tag{3b}$$

$$0.72 \leq \rho_{o0.66}/\rho_{o0.47} \leq 0.9 - 0.01(\Theta - 150°) \text{ THEN mixed} \tag{3c}$$

for scattering angles $\Theta = 150°$ to 168°. For scattering angles <150°, Θ is simply set to 150° for the boundary to collapse to 0.9 in that angle range. If the aerosol is mixed, then the fraction that the fine mode contributes to the total optical thickness, $\eta = \tau^f/\tau^{tot}$, is given by

$$\eta = 1 - \frac{\left[\dfrac{\rho_{o0.66}}{\rho_{o0.47}} - 0.72\right]}{0.90\text{-}0.01(\Theta\text{-}150°) - 0.72}, \tag{4}$$

again, where Θ is set to 150° when $\Theta < 150°$. Equation (4) gives an approximation to the fine-mode fraction over land. Its accuracy is dependent on the assumptions of aerosol models and surface reflectances. Furthermore, Eq. (4) magnifies relative errors in the retrievals of individual path radiances ($\rho_{o\,0.47}$, $\rho_{o\,0.66}$) by up to 4 to 8 times the original percentages. This is especially pronounced for situations of low aerosol loading. As a rule, satellite retrievals of aerosol optical thickness are more robust than corresponding retrievals of aerosol size, and retrievals of size parameter require sufficient aerosol loading in order to be valid (Ignatov et al. 1998; Remer et al. 2002).

In practice the "mixed" aerosol criterion [Eq. (3c)] is seldom found, and η is usually either 0 or 1 over land. However, in a monthly mean analysis, at least qualitatively, the pattern of fine-mode fraction corresponds to the global distributions of dust and nondust sources and transport. Figure 2 shows four monthly mean values of the fraction of total aerosol optical thickness attributed to the "nondust" aerosol model. Red shades indicate that "nondust" dominates over the monthly mean. Purple shades indicate that "pure dust" dominates. Blank areas in black are where no retrievals were made due to overly bright surfaces, monthly domination by clouds, or snow. Note that these plots do not differentiate between high and low aerosol loading. Sensitivity to aerosol size decreases in very clean regions.

Note that nondust is a misnomer because even though the nondust aerosol models are dominated by their fine modes, each also contains a coarse mode as well. Three nondust models are available and are described in Table 1, along with a description of the continental model and the dust model. The urban/industrial model remains unchanged from Kaufman et

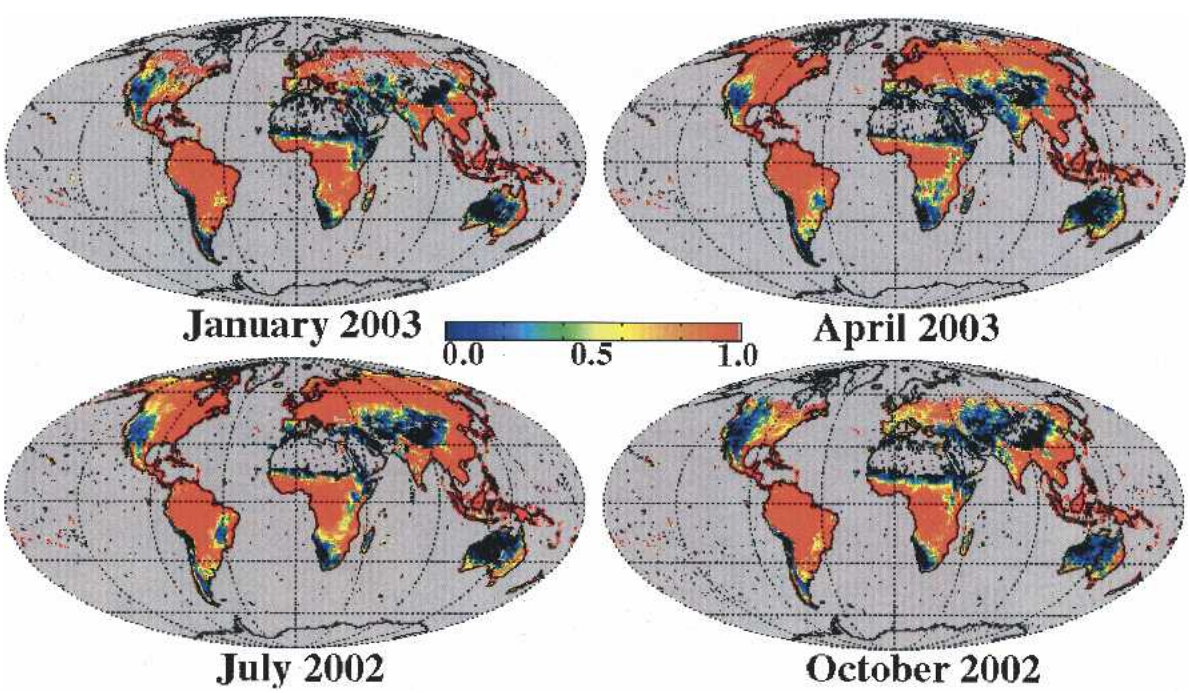

FIG. 2. Monthly mean plots of fraction of total aerosol optical thickness attributed to nondust or fine-mode aerosol over land. Fraction 1.0 indicates all fine mode. Fraction of 0.0 indicates all coarse mode.

al. (1997a) and Remer and Kaufman (1998). The new developing world—moderate absorption model is based on the biomass burning model of Kaufman et al. (1997a) and Remer et al. (1998), slightly modified to reflect the more recent study of Dubovik et al. (2002a). The developing world—heavy absorption model uses the same size parameters as the other developing world model, but allows for the greater aerosol light absorption noted in Africa (Ichoku et al. 2003; Eck et al. 2003; Dubovik et al. 2002a). Similar to the original conception of the algorithm, the current version uses season and geography to choose between the three nondust models (Dubovik et al. 2002a). However, the boundaries have changed. Figure 3 gives the new distribution of the three nondust models.

If the aerosol is identified as dust by Eq. (3), then the dust model of Table 1 is used. However, pure dust poses a problem with the dark target method. The assumption that $\rho_{2.13}$ is transparent to aerosols and provides direct information from the surface does not hold when the aerosol is composed of large particles. Therefore, Eq. (1) is not expected to hold in the pure dust case for very dark surfaces. However, over moderately bright surfaces, near the point of critical reflectance (Kaufman 1989) the surface contribution is negligible and the procedure can continue with minimal uncertainty introduced from the surface. Therefore, in the pure dust case retrievals are made only when $\rho_{2.13}$ falls between 0.15 and 0.25.

4) Determining aerosol optical thickness

In both the nondust and pure dust cases, the estimated surface reflectances ($\rho^s_{0.47}$, $\rho^s_{0.66}$) and the measured mean top-of-atmosphere reflectances ($\overline{\rho}_{0.47}$, $\overline{\rho}_{0.66}$) are used as input into the chosen model's LUT to retrieve values for the aerosol optical thicknesses, fluxes and other parameters. A full second retrieval is made from the appropriate model's LUT. This second full retrieval differs from Kaufman et al. (1997a) that describes, instead, a correction based on the single scattering approximation to the preliminary continental model retrieval described above. The final step in the process is to interpolate the values at 0.47 and 0.66 μm using an Ångström law in order to report optical thickness and flux values at 0.55 μm. Note that the algorithm does not retrieve aerosol directly at 0.55 μm over land because there is no established relationship between that channel and the surface reflectance at 2.13 μm analogous to Eq. (1) and, therefore, no method for estimating surface reflectance at 0.55 μm. However, 0.55 μm is an important wavelength often used in global climate modeling and analysis, and therefore MODIS reports a value for that wavelength even though there is no direct retrieval.

5) Alternative for bright surfaces

The standard dark target retrieval path, described above, that uses specific aerosol models requires a

TABLE 1. Size distribution parameters and single scattering albedo used in the MODIS lookup table for the land algorithm.

Mode	r_g(μm)	r_v(μm)	σ	V_o(μm)	ω_o(470)	ω_o(660)
			Continental aerosol model			
Water soluble	0.005	0.176	1.09	3.05	0.96	0.96
Dustlike	0.50	17.6	1.09	7.364	0.69	0.69
Soot	0.0118	0.050	0.693	0.105	0.16	0.16
			Urban/industrial			
Accumulation 1	0.036	0.106	0.6	F1	0.96	0.96
Accumulation 2	0.114	0.21	0.45	F2	0.97	0.97
Coarse 1	0.99	1.3	0.3	F3	0.92	0.92
Coarse 2	0.67	9.5	0.94	0.045	0.88	0.88
			Developing world—moderate absorption			
Accumulation	0.061	0.13	0.50	F4	0.91	0.89
Coarse	F5	F6	F7	F8	0.84	0.84
			Developing world—strong absorption			
Accumulation	0.061	0.13	0.50	F4	0.86	0.85
Coarse	F5	F6	F7	F8	0.84	0.84
			Desert dust			
Mode 1	0.0010	0.0055	0.755	6.0×10^{-8}	0.015	0.015
Mode 2	0.0218	1.230	1.160	0.01	0.95	0.95
Mode 3	6.24	21.50	0.638	0.006	0.62	0.62

F1: $-0.015 + 0.51\ \tau_{660} - 1.46\ \tau_{660}^2 + 1.07\ \tau_{660}^3$.
F2: $0.0038 - 0.086\ \tau_{660} + 0.90\ \tau_{660}^2 - 0.71\ \tau_{660}^3$.
F3: $-0.0012 + 0.031\ \tau_{660}$.
F4: $-0.0089 + 0.31\ \tau_{660}$.
F5: $1.0 - 1.3\ \tau_{660}$.
F6: $6.0 - 11.3\ \tau_{660} + 61\ \tau_{660}^2$.
F7: $0.69 + 0.81\ \tau_{660}$.
F8: $0.024 - 0.063\ \tau_{660} + 0.37\ \tau_{660}^2$.

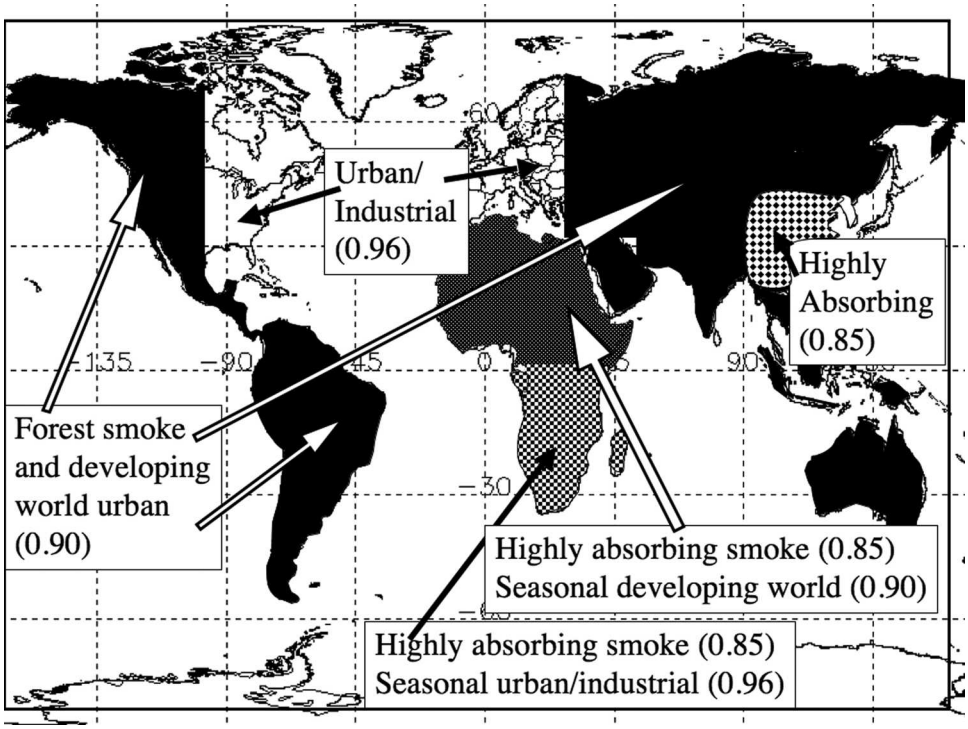

FIG. 3. Distribution of the nondust models used in the derivation of aerosol over land. Single scattering albedo values given in parentheses. Uncolored regions use the urban/industrial aerosol model. Solid black regions use the moderate absorption aerosol model all year. Large checkerboard pattern in East Asia denotes a region of strong absorption aerosol model all year. Africa is divided by region and season. North of the equator, during the burning season (Nov–May) the strong absorption aerosol model is used, while the moderate absorption model is used the remainder of the year. South of the equator, the burning season shifts to Jun–Oct when the strong absorption model is used, while in the remainder of the year the algorithm uses the urban/industrial model.

minimum of 12 dark pixels in every 20 × 20 pixel nominal 10-km box. Path B, of Fig. 1, represents an alternative if the surface is too bright to support 12 dark pixels in the standard manner. The upper limit of the $\rho_{2.13}$ value is permitted to increase as a function of the slant path until a final upper bound of $\rho_{2.13} = 0.40$ is reached. When the sun is at zenith and the satellite view nadir, path B collapses back to path A requirements. However, as the photon path increases, more and more signal originates from the atmosphere, and the contribution from the surface reflectance becomes less and less important. This is especially true at the 0.47-μm channel where atmospheric signal is highest and the surface usually darkest. For this reason, the alternative path B retrieves aerosol only in the 0.47-μm channel. At least 12 pixels must again meet the path B criteria, otherwise the procedure ends with no retrieval made, and fill values are placed in the output fields. Path B is considered to be less accurate than path A, and the quality control (QC) is set to 0, representing "poor quality." Because of the greater uncertainty over these brighter surfaces and because we retrieve in only one wavelength and cannot use the path radiance ratio to distinguish between dust and nondust aerosol, only the continental model is used in the retrieval. The aerosol optical thickness and flux are derived from the LUT for 0.47 μm. These parameters are extrapolated to 0.55 and 0.66 μm using the spectral dependence of the continental model.

Figure 4 shows a scene from the eastern part of southern Africa, where the surface reflectance is moderately bright. The top panel shows the MODIS retrieval of aerosol optical thickness at 0.55 μm following path A of the algorithm, which insists on 12 dark target pixels. The bottom panel shows the modified version of the algorithm, which allows retrievals over brighter surfaces by following both path A and path B. From the image we see how the extension to brighter surfaces fills in holes without introducing suspicious artifacts. In this example, permitting path B increases the number of retrievals over land from 7060 to 17 849. As we extend to brighter surfaces, we move away from the biomass burning regions into cleaner regions. Thus the mean optical thickness of the granule decreases from 0.20 to 0.15, but the standard deviation of the optical thickness remains constant at 0.15. For the 285 granules collected over southern Africa during the Southern African Regional Science Initiative (SAFARI

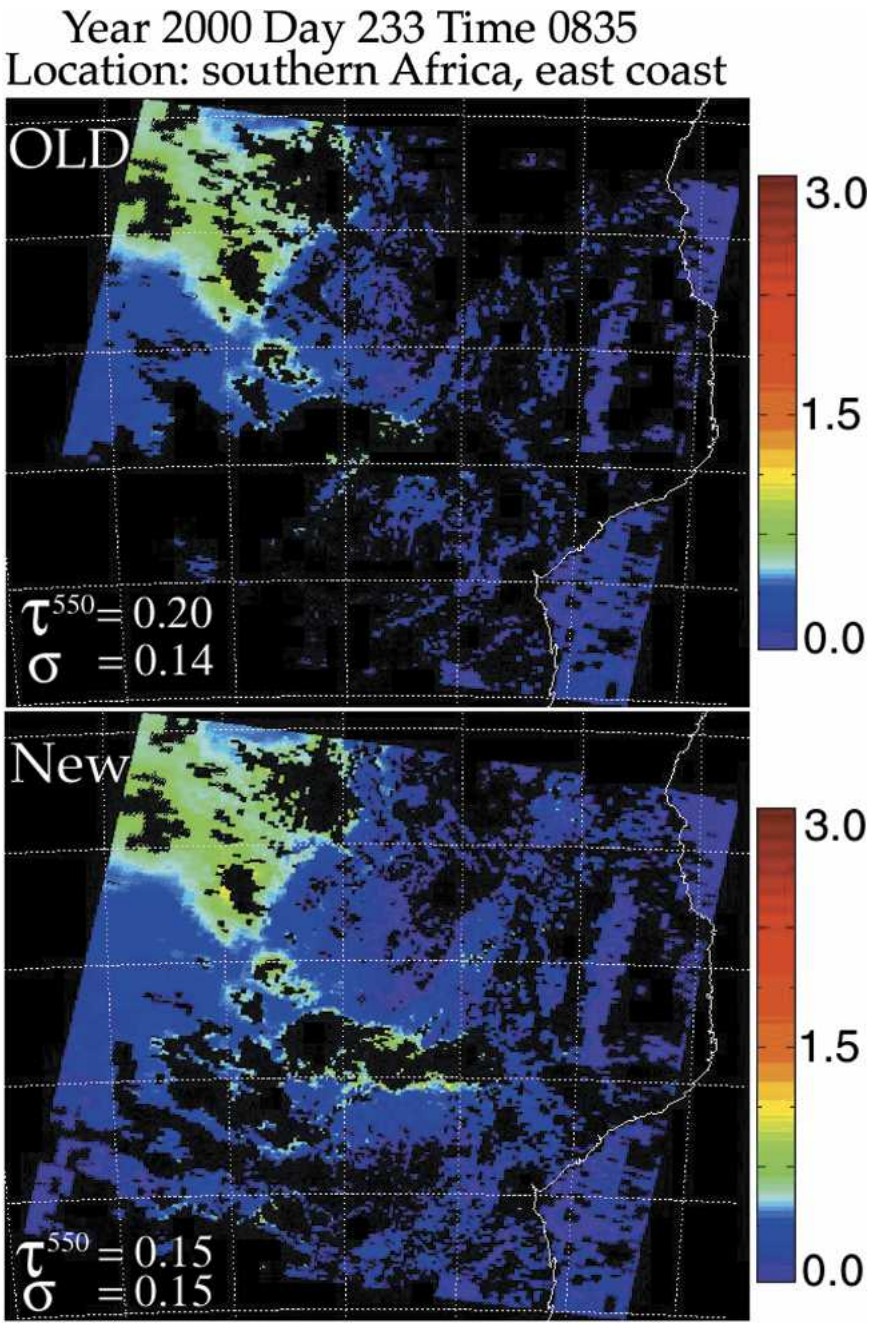

FIG. 4. MODIS-derived aerosol optical thickness at 0.55 μm for an image of the east coast of southern Africa. (top) The traditional dark target method described by path A in Fig. 1 is used. (bottom) The results after extending the retrieval to brighter surfaces as described by path B of Fig. 1. By extending to brighter surfaces the number of retrievals over land in this image increases from 7060 to 17 849.

2000) campaign (Swap et al. 2003), extending to brighter surfaces increases the number of land retrievals by 130%.

b. The ocean algorithm

The mechanics of the ocean algorithm are illustrated in Fig. 5. Although the core inversion remains similar to the process described in Tanré et al. (1997), the masking of clouds and sediments, the special handling of heavy dust including dust retrievals over glint, and revisions of the lookup table are new. As in the land algorithm, after the water vapor, ozone, and carbon dioxide corrections are applied, the first step in the ocean algorithm is to organize the reflectance

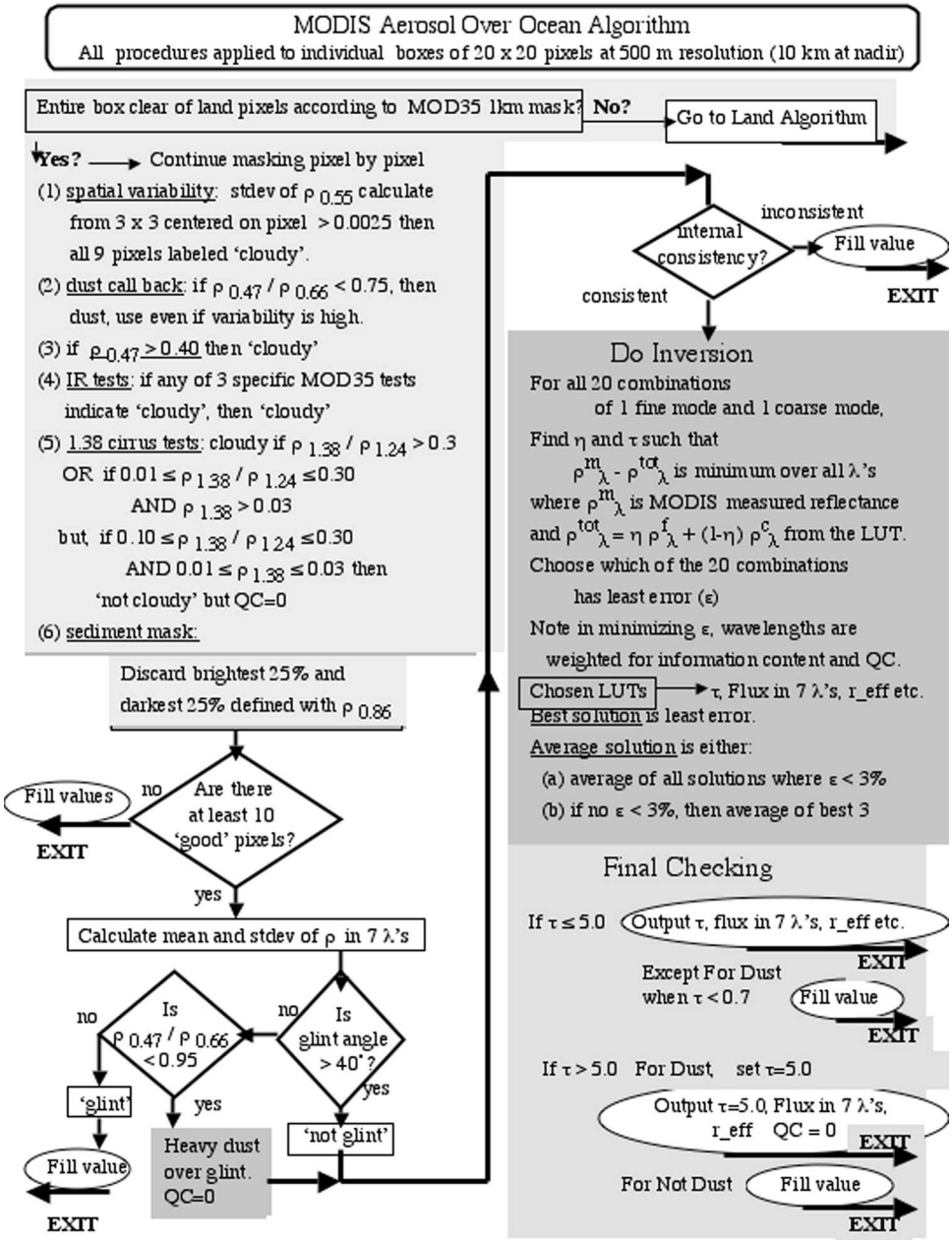

FIG. 5. Flowchart illustrating the derivation of aerosol over ocean.

from the six wavelengths used in the procedure ($\rho_{0.55}$, $\rho_{0.66}$, $\rho_{0.86}$, $\rho_{1.24}$, $\rho_{1.6}$, $\rho_{2.13}$) into nominal 10-km boxes of 20 × 20 pixels at 500-m resolution. This requires degrading the resolution of the 250-m channels ($\rho_{0.66}$ and $\rho_{0.86}$). The ocean algorithm requires all 400 pixels in the box to be identified as ocean pixels by the MOD/MYD35 mask. This helps to minimize problems introduced by shallow water near the coasts. If any land is encountered, the entire box is left for the land algorithm, but quality is decreased for coastal land retrievals.

1) CLOUD AND SEDIMENT MASKING

If all 400 pixels in the box are identified as water pixels, the algorithm then begins the arduous task of separating "good" pixels from "cloudy" pixels. The standard MOD35 cloud mask includes using the brightness in the visible channels to identify clouds. This procedure will mistake heavy aerosol as "cloudy" and miss retrieving important aerosol events over ocean. On the other hand, relying on IR tests alone permits low-altitude, warm clouds to escape and be misidentified as

"clear," introducing cloud contamination in the aerosol products. Thus, our primary cloud mask is based on the difference in spatial variability between aerosols and clouds (Martins et al. 2002). The algorithm marches through the 10 km × 10 km box, examining the standard deviation of $\rho_{0.55}$ in every group of 3 × 3 pixels. Any group of nine pixels with standard deviation greater than 0.0025 is labeled as "cloudy," and all nine pixels in the group are discarded (Martins et al. 2002). The only exception to this rule is for heavy dust, which may at times be as spatially inhomogeneous as clouds. Heavy dust is identified by its absorption at 0.47 μm using the ratio ($\rho_{0.47}/\rho_{0.66}$). This quantifies the difference that our eyes witness naturally. Dust absorbs at blue wavelengths and appears brown. Clouds are spectrally neutral and appear white to our eyes. If $\rho_{0.47}/\rho_{0.66} < 0.75$, then the central pixel of the group of nine is identified as "dust" and will be included in the retrieval even if it is inhomogeneous. This is a conservative threshold that requires very heavy dust in order to avoid clouds. Less restrictive thresholds would permit more dust retrievals, but might accidentally permit cloud contamination.

The spatial variability test separates aerosol from most cloud types, but sometimes fails at the centers of large, thick clouds and also with cirrus, both of which can be spatially smooth. The centers of large, thick clouds are very bright in the visible, so we identify these clouds when $\rho_{0.47} > 0.40$. This is an extremely high threshold that could be a nonabsorbing aerosol optical thickness greater than 5.0, but only for nonabsorbing aerosol. Absorbing aerosol never produces that high value of reflectance and will pass this cloud test unscathed. Some high values of nonabsorbing aerosol may be discarded along with bright clouds, but this confusion is rare. Heavy aerosol loading, with $\tau > 5.0$, absorbs somewhat at 0.47 μm and fails to reach the 0.40 threshold value exhibited by very bright white clouds.

Cirrus clouds are identified with a combination of infrared and near-infrared tests. Three infrared tests provided by the standard MODIS cloud mask, MOD35, are examined. These tests are IR cirrus test (byte 2, bit 4), 6.7-μm test (byte 2, bit 8), and Delta IR test (byte 3, bit 3) (Ackerman et al. 1998). If any one of the three tests indicates clouds, we label the pixel as "cloudy." The near-infrared cirrus test is based on the reflectance in the 1.38-μm channel and the ratio $\rho_{1.38}/\rho_{1.24}$ (Gao et al. 2002). It is applied in the algorithm as a three-step process:

IF ($\rho_{1.38}/\rho_{1.24} > 0.3$) THEN "cloudy"

IF ($0.10 \leq \rho_{1.38}/\rho_{1.24} \leq 0.30$) AND ($\rho_{1.38} > 0.03$)

AND ($\rho_{0.66} > 1.5\rho_{0.66}^{\text{Rayleigh}}$)

THEN "cloudy"

IF ($0.10 \leq \rho_{1.38}/\rho_{1.24} \leq 0.30$) AND ($0.01 \leq \rho_{1.38} \leq 0.03$)

AND ($\rho_{0.66} > 1.5\rho_{0.66}^{\text{Rayleigh}}$)

THEN "not cloudy", but the quality of the retrieval

is "poor" (QC = 0).

IF ($\rho_{0.66} < 1.5\ \rho_{0.66}^{\text{Rayleigh}}$) OR ($\rho_{1.38} < 0.01$)

AND NOT ($\rho_{1.38}/\rho_{1.24} > 0.3$)

THEN "not cloudy", and the quality of the retrieval

is "good" (QC = 3).

A quality flag of QC = 0 permits a retrieval at the orbital level (level 2), but prohibits the retrieval from contributing to the long-term global aerosol statistics (level 3). Only retrievals with QC > 0 contribute to the level 3 quality weighted products.

The final mask applied to the data is the sediment mask, which identifies which ocean scenes are contaminated by river sediments (Li et al. 2003), discarding those pixels. The sediment mask takes advantage of the strong absorption by water at wavelengths longer than 1 μm. Spectral reflectances over water with suspended sediments show elevated values in the visible, but not in the longer wavelengths. This is a spectral signature that is quite different from clear ocean water and also different from airborne dust.

All pixels that have evaded the cloud mask tests and the sediment mask are sorted according to their $\rho_{0.86}$ value. The darkest and brightest 25% are discarded, thereby leaving the middle 50% of the data. The filter is used to eliminate residual cloud contamination, cloud shadows, or other unusual extreme conditions in the box. Because the ocean cloud mask and the ocean surface are expected to be more accurate than their counterparts over land, the filter is less restrictive than the one used in the land retrieval. Of the 400 pixels in the original box, at least 10 must remain for the 0.86-μm channel after the masking and filtering. Otherwise, no retrieval is attempted and all aerosol products in the 10-km box are given fill values. If there are at least 10 good pixels, the mean reflectance and standard deviation are calculated for the remaining good pixels at the six pertinent wavelengths.

2) Ocean glint and internal consistency

The glint angle is defined as

$$\Theta_{\text{glint}} = \cos^{-1}[(\cos\theta_s \cos\theta_v) + (\sin\theta_s \sin\theta_v \cos\phi)], \quad (5)$$

where θ_s, θ_v, and ϕ are the solar zenith, the satellite zenith, and the relative azimuth angles (between the sun and satellite), respectively (Levy et al. 2003). Note that Fresnel reflection corresponds to $\Theta_{\text{glint}} = 0$. The ocean algorithm was designed to retrieve only over dark ocean, away from glint (except in one special case described below). If $\Theta_{\text{glint}} > 40°$, we can avoid glint contamination and proceed with the retrieval. The algorithm performs several consistency checks of the spectral reflectances. Depending on the outcome of these consistency checks, the algorithm may either declare the reflectances to be beyond the range necessary

for a successful inversion and exit the procedure or continue onto the inversion after assigning quality flags (QC values) to each wavelength.

3) INVERSION PROCEDURE

The inversion procedure is aptly described in Tanré et al. (1997) and Levy et al. (2003). Following Tanré et al. (1996), we know that the six reflectances measured from MODIS and used in the ocean retrieval (0.55–2.13 μm) contain three pieces of information about the aerosol. From this information we derive three parameters: the optical thickness at one wavelength ($\tau_{0.55}^{\mathrm{tot}}$), the reflectance weighting parameter at one wavelength ($\eta_{0.55}$), and the effective radius, which is the ratio of the third and second moments of the aerosol size distribution. The inversion is based on a LUT that now consists of four fine modes and five coarse modes [Table 2, following Levy et al. (2003), which differs from the 11 possible modes listed in Tanré et al. (1997)]. The LUT is constructed using the radiative transfer code of Ahmad and Fraser (1982). It consists of the top-of-atmosphere reflectances in six wavelengths calculated for a variety of geometries, a rough ocean surface with nonzero water-leaving radiance only at 0.55 μm ($\rho_{0.55}^{\mathrm{s}} = 0.005$), and several values of $\tau_{0.55}^{\mathrm{tot}}$ for each single-mode aerosol model of Table 2. Note that the LUT is defined in terms of a single wavelength of optical thickness. However, the parameters of each of the single mode models define a unique spectral dependence for that model, which can be applied to the retrieved value of $\tau_{0.55}^{\mathrm{tot}}$ to determine optical thickness at other wavelengths. Table 3 gives the spectral dependence of extinction, asymmetry parameter, and single scattering albedo for each of the modes of Table 2.

The procedure requires both a fine mode and a coarse mode for each retrieval. The modes from the LUT are combined using η as the weighting parameter,

$$\rho_\lambda^{\mathrm{LUT}}(\tau_{0.55}^{\mathrm{tot}}) = \eta\rho_\lambda^{\mathrm{f}}(\tau_{0.55}^{\mathrm{tot}}) + (1 - \eta)\rho_\lambda^{\mathrm{c}}(\tau_{0.55}^{\mathrm{tot}}). \qquad (6)$$

Equation (6) means that the spectral reflectance measured from the satellite that corresponds to the LUT value, $\rho_\lambda^{\mathrm{LUT}}(\tau_{0.55}^{\mathrm{tot}})$ for the determined values of η and $\tau_{0.55}^{\mathrm{tot}}$, is a weighted average of the reflectance values for an atmosphere with a pure fine mode "f" and optical thickness $\tau_{0.55}^{\mathrm{tot}}$ and the reflectance of an atmosphere with a pure coarse mode "c" also with the same $\tau_{0.55}^{\mathrm{tot}}$. In appendix A, we show that $\eta = \tau_{0.55}^{\mathrm{f}}/\tau_{0.55}^{\mathrm{tot}}$, the fraction of total optical thickness at 0.55 μm contributed by the fine mode.

For each of the 20 combinations of one fine mode and one coarse mode, the inversion finds the pair of $\tau_{0.55}^{\mathrm{tot}}$ and $\eta_{0.55}$ that minimizes the error (ε) defined as

$$\varepsilon = \sqrt{\frac{\sum_{\lambda=1}^{6} N_\lambda \left(\frac{\rho_\lambda^{\mathrm{m}} - \rho_\lambda^{\mathrm{LUT}}}{\rho_\lambda^{\mathrm{m}} + 0.01}\right)^2}{\sum_{\lambda=1}^{6} N_\lambda}}, \qquad (7)$$

where N_λ is the sum of good pixels at wavelength λ, $\rho_\lambda^{\mathrm{m}}$ is the measured MODIS reflectance at wavelength λ, and $\rho_\lambda^{\mathrm{LUT}}$ is calculated from the combination of modes in the lookup table and is defined by Eq. (6). The 0.01 prevents a division by zero for the longer wavelengths under clean conditions (Tanré et al. 1997). Here, $\rho_{0.87}^{\mathrm{LUT}}$ is required to exactly fit the MODIS observed reflectance at that wavelength. The best fits to the other five wavelengths are found via Eq. (7). We choose the 0.87-μm channel to be the primary wavelength because it is less affected by variability in water-leaving radiances than the shorter wavelengths, yet still exhibits a strong aerosol signal, even for aerosols dominated by the fine mode. By emphasizing accuracy in this channel, variability in chlorophyll will have negligible effect on the optical thickness retrieval and minimal effect on $\eta_{0.55}$.

The 20 solutions are then sorted according to values of ε. The best solution is the combination of modes with

TABLE 2. Refractive indices, median, standard deviation, and effective radius for the aerosol models used in the MODIS lookup table for the ocean algorithm. Models 1–4 are fine modes and models 5–9 are coarse modes. From Levy et al. (2003).

	λ = 0.47→0.86 μm	λ = 1.24 μm	λ = 1.64 μm	λ = 2.13 μm	r_g	σ	r_{eff}	Comments
1	1.45–0.0035*i*	1.45–0.0035*i*	1.43–0.01*i*	1.40–0.005*i*	0.07	0.40	0.10	Wet water soluble type
2	1.45–0.0035*i*	1.45–0.0035*i*	1.43–0.01*i*	1.40–0.005*i*	0.06	0.60	0.15	Wet water soluble type
3	1.40–0.0020*i*	1.40–0.0020*i*	1.39–0.005*i*	1.36–0.003*i*	0.08	0.60	0.20	Water soluble with humidity
4	1.40–0.0020*i*	1.40–0.0020*i*	1.39–0.005*i*	1.36–0.003*i*	0.10	0.60	0.25	Water soluble with humidity
5	1.45–0.0035*i*	1.45–0.0035*i*	1.43–0.0035*i*	1.43–0.0035*i*	0.40	0.60	0.98	Wet sea salt type
6	1.45–0.0035*i*	1.45–0.0035*i*	1.43–0.0035*i*	1.43–0.0035*i*	0.60	0.60	1.48	Wet sea salt type
7	1.45–0.0035*i*	1.45–0.0035*i*	1.43–0.0035*i*	1.43–0.0035*i*	0.80	0.60	1.98	Wet sea salt type
8	1.53–0.003*i* (0.47) 1.53–0.001*i* (0.55) 1.53–0.000*i* (0.66) 1.53–0.000*i* (0.86)	1.46–0.000*i*	1.46–0.001*i*	1.46–0.000*i*	0.60	0.60	1.48	Dustlike type
9	1.53–0.003*i* (0.47) 1.53–0.001*i* (0.55) 1.53–0.000*i* (0.66) 1.53–0.000*i* (0.86)	1.46–0.000*i*	1.46–0.001*i*	1.46–0.000*i*	0.50	0.80	2.50	Dustlike type

TABLE 3. Values of the normalized extinction coefficients, asymmetry parameter, single scattering albedo for the nine ocean models of Table 2.

Model	0.47 μm	0.55 μm	0.66 μm	0.87 μm	1.24 μm	1.61 μm	2.13 μm
Normalized extinction coefficients							
1	1.538	1.0	0.661	0.286	0.085	0.046	0.016
2	1.300	1.0	0.764	0.427	0.169	0.081	0.030
3	1.244	1.0	0.796	0.483	0.211	0.104	0.042
4	1.188	1.0	0.836	0.549	0.269	0.140	0.060
5	0.963	1.0	1.037	1.081	1.055	0.919	0.745
6	0.980	1.0	1.034	1.100	1.177	1.166	1.081
7	0.986	1.0	1.025	1.079	1.162	1.225	1.215
8	0.977	1.0	1.023	1.086	1.185	1.192	1.124
9	0.964	1.0	1.000	1.039	1.098	1.117	1.105
Asymmetry parameter							
1	0.5755	0.5117	0.4478	0.3221	0.1773	0.1048	0.0622
2	0.6832	0.6606	0.6357	0.5756	0.4677	0.3685	0.2635
3	0.7354	0.7183	0.6991	0.6510	0.5590	0.4715	0.3711
4	0.7513	0.7398	0.7260	0.6903	0.6179	0.5451	0.4566
5	0.7450	0.7369	0.7328	0.7316	0.7330	0.7411	0.7282
6	0.7770	0.7651	0.7503	0.7358	0.7314	0.7461	0.7446
7	0.8035	0.7912	0.7738	0.7506	0.7335	0.7443	0.7461
8	0.7534	0.7200	0.6979	0.6795	0.7129	0.7173	0.7190
9	0.7801	0.7462	0.7234	0.7065	0.7220	0.7176	0.7151
Single scattering albedo							
1	0.9735	0.9683	0.9616	0.9406	0.8786	0.5390	0.4968
2	0.9782	0.9772	0.9757	0.9704	0.9554	0.8158	0.8209
3	0.9865	0.9864	0.9859	0.9838	0.9775	0.9211	0.9156
4	0.9861	0.9865	0.9865	0.9855	0.9819	0.9401	0.9404
5	0.9239	0.9358	0.9451	0.9589	0.9707	0.9753	0.9774
6	0.8911	0.9026	0.9178	0.9377	0.9576	0.9676	0.9733
7	0.8640	0.8770	0.8942	0.9175	0.9430	0.9577	0.9669
8	0.9013	0.9674	1.0000	1.0000	1.0000	1.0000	1.0000
9	0.8669	0.9530	1.0000	1.0000	1.0000	1.0000	1.0000

the accompanying $\tau_{0.55}^{\mathrm{tot}}$ and $\eta_{0.55}$ that minimizes ε. The solution may not be unique. The average solution is the average of all solutions with $\varepsilon < 3\%$, or if no solution has $\varepsilon < 3\%$, then the average is of the three best solutions. Once the solutions are found, then the chosen combination of modes is the de facto derived aerosol model. A variety of parameters can be inferred from the chosen size distribution including spectral optical thickness, effective radius, spectral flux, mass concentration, etc.

4) NOTE ON ERRORS

Tanré et al. (1997) explore the sensitivity of the inversion procedure to various sources of error. For example, they tested the retrieval sensitivity by introducing a random calibration error of 1%, finding no systematic bias and negligible impact upon the optical thickness retrievals. The effects on the retrieved size parameters were much greater. Errors due to the 1% calibration error translated to uncertainties of ± 0.25 for $\eta_{0.55}=1$ and ± 0.50 for $\eta_{0.55}=0$. For small particles less than 0.40 μm, the effective radius was retrieved to within ± 0.10 μm, but for large particles greater than 1.0 μm the effective radius was severely underestimated. Since that sensitivity study, the lookup table has been changed and the number of possible aerosol models available to the inversion has been reduced. With fewer choices, the inversion is less sensitive to calibration errors. We know now that the true uncertainty in the input reflectances is 1.8%–1.9% (Guenther et al. 2002), not the 1% assumed in the study. This will have little additional effect on the accuracy of the optical thickness retrievals, but may further reduce the accuracy of the size retrievals.

5) FINAL CHECKING

Before the final results are output, additional consistency checks are employed. In general, if the retrieved optical thickness at 0.55 μm is greater than -0.01 and less than 5, then the results are output. Negative optical depths are possible, occurring only in situations with low optical depth. This situation arises from errors in assumptions of surface conditions, aerosol properties, or calibration expectations. We choose to report small negative values in order not to introduce a positive bias in long-term statistics for clean marine conditions, but negative optical depths are given lower quality flags. Quality flags may be adjusted during this final checking phase.

6) SPECIAL CASE: HEAVY DUST OVER GLINT

If $\Theta_{\mathrm{glint}} \leq 40°$, then we check for heavy dust in the glint. Heavy dust has a distinctive spectral signature because

of light absorption at blue wavelengths. In the situation of identifying heavy dust over glint we designate all values of $\rho_{0.47}/\rho_{0.66} < 0.95$ to be heavy dust. If heavy dust is identified in the glint, the algorithm continues with the retrieval, although it sets QC = 0. This permits the retrieval, but prohibits the values from being included in the quality weighted level 3 statistics. If heavy dust is not identified in the glint, then the algorithm writes fill values to the aerosol product arrays and exits the procedure.

3. The aerosol products

Examples of the three main aerosol products are shown in Fig. 6, which shows heavy smoke aerosol produced by fires in Canada and transported in this image south across the mid-Atlantic region of the United States and out to sea. Shown are the visible true color image and the three main products including the land and ocean aerosol optical thickness at 0.55 μm ($\tau_{0.55}$), the fraction of the optical thickness contributed by the

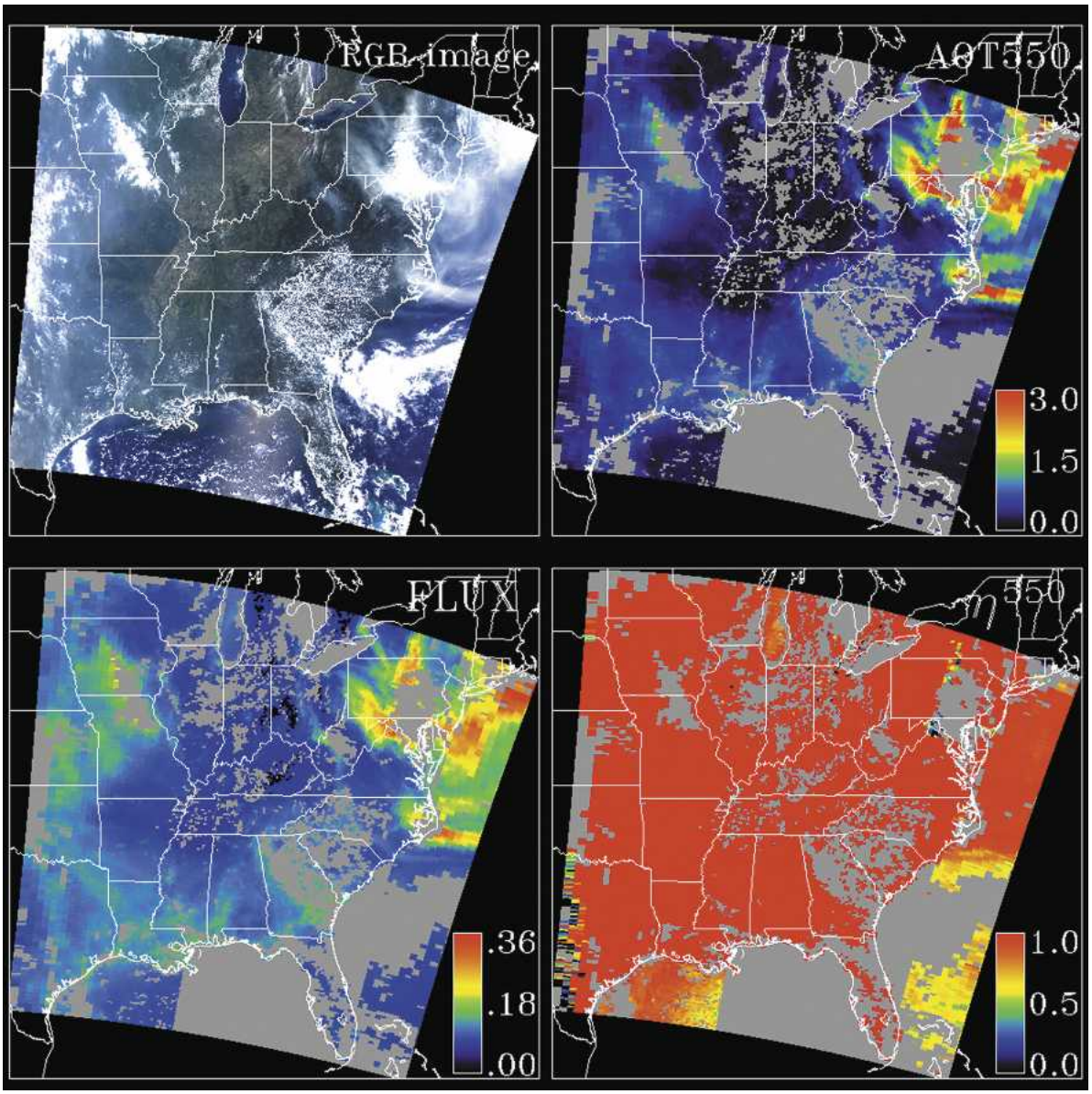

FIG. 6. Examples of MODIS aerosol products at the level 2 stage (MOD04). The data represent a 5-min granule collected on 7 Jul 2002 from 1835 to 1840 UTC when smoke from Canadian fires had been transported south over the mid-Atlantic states and then out to sea. (Upper left) A true color image created from level 1b reflectances, (upper right) aerosol optical thickness at 550 nm, (lower left) reflected flux at 550 nm, and (lower right) fraction of fine mode. The sun glint over the Gulf of Mexico can be seen in the true color red–green–blue (RGB) image. The other panels exhibit a sharp dividing boundary in this region due to the application of the glint mask.

fine mode ($\eta_{0.55}$), and the reflected flux at the top of the atmosphere at 0.55 μm. The flux is defined as the hemispherical irradiance at a particular wavelength. Over land, the flux is defined for zero surface reflectance and computed consistently with the same aerosol parameters used in the optical thickness retrieval. Over ocean, the flux is defined for the same rough ocean surface model and the same aerosol parameters derived in the optical thickness retrieval. Errors in the retrieved aerosol optical thickness that may be introduced by inaccurate assumptions of the aerosol model are subsequently canceled when those same aerosol model assumptions are used with the optical thickness to calculate top-of-atmosphere fluxes; errors introduced by assumptions of surface reflectance will remain. For a monthly average, the consistent calculations produce a highly accurate measure of the flux more accurate than the optical thickness itself.

Figure 6 shows orbital-based level 2 products cut from 5-min segments of a satellite orbit, called granules. The level 2 products, designated as MOD04 files, contain 64 separate products, all connected to the aerosol retrieval. The level 2 files are produced every day and represent the first level of MODIS aerosol retrieval. In addition, statistics based on the level 2 aerosol retrievals can also be found in level 3 files, designated as MOD08 files. These level 3 files contain parameters produced from the entire MODIS atmospheres team and include such parameters as water vapor and cloud characteristics along with the aerosol information. The level 3 data are averaged to a 1° latitude/longitude grid and are produced every day (MOD08_D3), averaged every 8 days (MOD08_E3) or averaged on a monthly basis (MOD08_M3). They include both statistics calculated equally from all the data, and also statistics weighted by the quality of each individual retrieval. Quality weights of 0 will prevent poor retrievals from affecting the calculated statistics of the quality weighted quantities. Further information about the level 3 products can be found in King et al. (2003) and online at http://modis-atmos.gsfc.nasa.gov.

All together there are 64 aerosol products at level 2: 9 products describe geometry and location, 3 products are joint land and ocean products, 23 are land-only products, and 29 are ocean-only products. Tables 4–7 lists all 64 products. The three joint land and ocean products are simple two-dimensional arrays of one wavelength (Fig. 6). The land-only and ocean-only products contain an additional dimension. In many cases this additional dimension is wavelength. Tables 4–7 list the wavelengths for each product where applicable. The additional dimension in the ocean-only products can designate either the "best" solution or the "average" solution from the ocean retrieval as described above in section 2b(3). Both solutions are reported for some parameters, although they are often identical.

Tables 4–7 also list whether the product is "validated," "not yet validated," "derived," "experimental," or "diagnostic." A validated product indicates that substantial comparison was made to ground-based data and that the retrieval is well characterized so that error bars can be defined and comfortably applied to the retrieval product (Ichoku et al. 2002; Chu et al. 2002; Remer et al. 2002). Examples of validation are shown in section 4. "Not yet validated" indicates that the retrieved parameter has not yet been well characterized, but that data are being collected and analysis is underway. "Derived" is a parameter that follows from the retrieval's choice of aerosol model and the magnitude of the retrieved optical thickness. Definitions of some of the derived parameters are given in appendix B. A derived parameter is not directly retrieved and there are no expectations of ever validating a derived parameter with independent data. "Experimental" is a scientific product that may have future applications but, as of now, is too innovative to be well characterized. "Diagnostic" refers to output that is either an auxillary or intermediate parameter. Diagnostic parameters are meant to aid in understanding the final product, but will never themselves become validated Recommendations for choosing particular products are given in appendix C.

TABLE 4. Contents of MODIS aerosol level 2 hdf file (MOD04): Time and geometric information. Two-dimensional arrays of 204 × 135 are indicated.

Name of product	Dimension	Status
Longitude	2D	Diagnostic
Latitude	2D	Diagnostic
Scan_Start_Time	2D	Diagnostic
Solar_Zenith	2D	Diagnostic
Solar_Azimuth	2D	Diagnostic
Sensor_Zenith	2D	Diagnostic
Sensor_Azimuth	2D	Diagnostic
Scattering_Angle	2D	Diagnostic
Cloud_Mask_QA	2D	Diagnostic

4. Validation of aerosol products

Our primary means of validation is comparison with equivalent measurements from Aerosol Robotic Network (AERONET) ground-based sun/sky radiometers (Holben et al. 1998). The AERONET instruments

TABLE 5. Contents of MODIS aerosol level 2 hdf file (MOD04): Global land and ocean products, at 550 nm.

Name of product	Dimension	Status
Optical_Depth_ Land_And_Ocean	2D	Validated
Optical_Depth_Ratio_ Small_Land_And_Ocean	2D	Not yet validated
Reflected_Flux_ Land_And_Ocean	2D	Derived

TABLE 6. Contents of MODIS aerosol level 2 hdf file (MOD04): Land products.

Name of product	Dimension	Status
Corrected_Optical_Depth_Land	0.47, 0.55, 0.66 μm	Validated
Optical_Depth_Ratio_Small_Land	0.55 μm	Not yet valid
Mass_Concentration_Land	2D	Derived
Ångström_Exponent_Land	0.66/0.47	Not yet valid
Reflected_Flux_Land	0.47, 0.55, 0.66 μm.	Derived
Transmitted_Flux_Land	0.47, 0.66 μm	Derived
Aerosol_Type_Land	2D	Diagnostic
Continental_Optical_Depth_Land	0.47, 0.66 μm	Diagnostic
Estimated_Uncertainty_Land	0.47, 0.66 μm	Diagnostic
Mean_Reflectance_Land_All	0.47, 0.66, 2.13 μm	Diagnostic
Standard_Deviation_Reflectance_Land_All	0.47, 0.66, 2.13 μm	Diagnostic
Cloud_Fraction_Land	2D	Diagnostic
Number_Pixels_Percentile_Land	0.47, 0.66 μm	Diagnostic
Mean_Reflectance_Land	0.47, 0.66, 0.87, 2.13, 3.75 μm	Diagnostic
STD_Reflectance_Land	0.47, 0.66, 0.87, 2.13, 3.75μm	Diagnostic
Quality_Assurance_Land	See QA plan	Diagnostic
Path_Radiance_Land	0.47, 0.66 μm	Experimental
Error_Path_Radiance_Land	0.47, 0.66 μm	Diagnostic
Critical_Reflectance_Land	0.47, 0.66 μm	Experimental
Error_Critical_Reflectance_Land	0.47, 0.66 μm	Diagnostic
Quality_Weight_Path_Radiance	0.47, 0.66 μm	Experimental
Quality_Weight_Critical_Reflectance_Land	0.47, 0.66 μm	Experimental
Quality_Assurance_Crit_Ref_Land	0.47, 0.66, 0.87, 2.13, 3.75 μm	Diagnostic

measure spectral aerosol optical thickness, τ_λ to within ~0.01 for the channels 0.38, 0.44, 0.50, 0.67, 0.87, and 1.02 μm (Eck et al. 1999). They also can derive ambient, total atmospheric column aerosol effective radius, r_{eff}, whenever conditions are favorable (Dubovik et al. 2000). The methodology of comparing temporally varying AERONET data with spatially varying MODIS data is described in Ichoku et al. (2002). In the follow-

TABLE 7. Contents of MODIS aerosol level 2 hdf file (MOD04): Ocean products.

Name of product	Dimension	Status
Effective_Optical_Depth_Average_Ocean	0.47, 0.55, 0.66, 0.87 1.24, 1.63, 2.13 μm	Validated
Optical_Depth_Small_Average	0.47, 0.55, 0.66, 0.87 1.24, 1.63, 2.13 μm	Not yet validated
Optical_Depth_Large_Average	0.47, 0.55, 0.66, 0.87 1.24, 1.63, 2.13 μm	Not yet validated
Effective_Radius_Ocean	Best, average	Validated
Optical_Depth_Ratio_Small_Ocean_0.86micron	Best, average	Not yet validated
Mass_Concentration_Ocean	Best, average	Derived
Cloud_Condensation_Nuclei_Ocean	Best, average	Derived
Ångström_Exponent_1_Ocean	0.55/0.87	Not yet validated
Ångström_Exponent_2_Ocean	0.87/2.13	Not yet validated
Reflected_Flux_Average_Ocean	0.47, 0.55, 0.66, 0.87 1.24, 1.63, 2.13 μm	Derived
Transmitted_Flux_Average_Ocean	0.47, 0.55, 0.66, 0.87 1.24, 1.63, 2.13 μm	Derived
Asymmetry_Factor_Average_Ocean	0.47, 0.55, 0.66, 0.87 1.24, 1.63, 2.13 μm	Derived
Backscattering_Ratio_Average_Ocean	0.47, 0.55, 0.66, 0.87 1.24, 1.63, 2.13 μm	Derived
Solution_Index_Ocean_Small	Best, average	Diagnostic
Solution_Index_Ocean_Large	Best, average	Diagnostic
Least_Squares_Error_Ocean	Best, average	Diagnostic
Optical_Depth_by_models_Ocean	Nine models	Diagnostic
Effective_Optical_Depth_Best_Ocean	0.47, 0.55, 0.66, 0.87 1.24, 1.63, 2.13 μm	Diagnostic
Optical_Depth_Small_Best	0.47, 0.55, 0.66, 0.87 1.24, 1.63, 2.13 μm	Diagnostic
Optical_Depth_Large_Best	0.47, 0.55, 0.66, 0.87 1.24, 1.63, 2.13 μm	Diagnostic
Reflected_Flux_Best_Ocean	0.47, 0.55, 0.66, 0.87 1.24, 1.63, 2.13 μm	Diagnostic
Transmitted_Flux_Best_Ocean	0.47, 0.55, 0.66, 0.87 1.24, 1.63, 2.13 μm	Diagnostic
Asymmetry_Factor_Best_Ocean	0.47, 0.55, 0.66, 0.87 1.24, 1.63, 2.13 μm	Diagnostic
Backscattering_Ratio_Best_Ocean	0.47, 0.55, 0.66, 0.87 1.24, 1.63, 2.13 μm	Diagnostic
Cloud_Fraction_Ocean	2D	Diagnostic
Number_Pixels_Used_Ocean	2D	Diagnostic
Mean_Reflectance_Ocean	0.47, 0.55, 0.66, 0.87 1.24, 1.63, 2.13 μm	Diagnostic
STD_Reflectance_Ocean	0.47, 0.55, 0.66, 0.87 1.24, 1.63, 2.13 μm	Diagnostic
Quality_Assurance_Ocean	See QA plan	Diagnostic

ing validation, we use AERONET level 1.5 data, which are cloud screened but not quality assured, primarily because final calibration is not applied (Smirnov et al. 2000). The procedure that collocates MODIS and AERONET data is applied during a very short window of opportunity (~24 h) after the operational MODIS aerosol product has been processed and before that data are transferred to the archive. The data are purged from the operational facility after transfer. Level 2.0 AERONET data become available only several months behind real time depending on site. During a system-wide reprocessing of MODIS data, which may take place months to years after real time, if AERONET level 2.0 data are available then, they are extracted and added to the MODIS validation dataset. The two years of collocated data in this analysis do not benefit from reprocessing and are therefore taken from the real-time processing that use AERONET level 1.5. Figure 7 shows the distribution of the 132 AERONET stations used in the comparisons to be described below. Although North American and European stations dominate the database, all continents (except Antarctica), all oceans, and all aerosol types are represented.

Validation is an ongoing effort. Not only do aerosol conditions vary in location and time, requiring a continued effort to validate the algorithms under various conditions, but the algorithms themselves evolve. The algorithms' development and history, starting from the most recent version and going backward in time can be found at the MODIS atmospheres Web site (http://modis-atmos.gsfc.nasa.gov/MOD04_L2/history.html). Much of the algorithm modifications concern experimental products, improved cloud/snow/water masking, internal bookkeeping, or minor adjustments meant to improve long-term statistics. However, the last adjustment over land to version 4.2.1 modifies the land lookup tables to increase aerosol absorption as needed in certain regions (Ichoku et al. 2003). This is a significant change, which will not be reflected in the validation plots described below.

A preliminary validation of the aerosol products was made of the data collected in the first months of operation. The results are reported in Ichoku et al. (2002), Chu et al. (2002), and Remer et al. (2002). The preliminary validation compared 2–3 months of MODIS aerosol optical thickness and effective radius retrievals to the same parameters observed (optical thickness) or derived (effective radius) from AERONET radiometers. The preliminary validation from the limited dataset showed the MODIS-derived parameters agreed with the AERONET parameters to within the expected prelaunch uncertainties: $\pm 0.05 \pm 0.15\tau$ for optical thickness over land, and $\pm 0.03 \pm 0.05\ \tau$ for optical thickness and $\pm 25\%$ for effective radius over ocean.

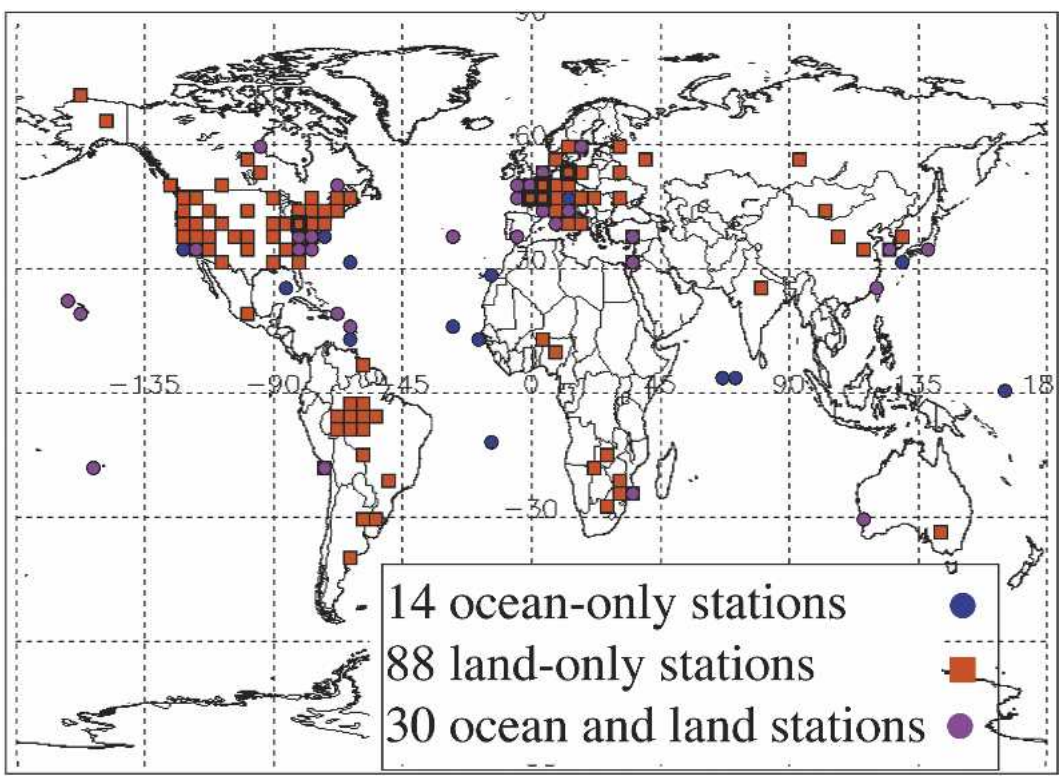

FIG. 7. The distribution of the 132 AERONET stations used to validate MODIS land and ocean aerosol retrieval algorithms.

a. Validation of aerosol optical thickness

1) VALIDATION OVER LAND

At the time of this analysis there were two years of MODIS aerosol products collocated with AERONET retrievals (1 August 2000 to 1 August 2002). Figure 8 shows plots of 5906 collocated points over land at wavelengths 0.47, 0.55, and 0.66 μm. There are no AERONET measurements at the MODIS wavelengths of 0.47 and 0.55 μm; therefore, the AERONET values in the plots of Fig. 8 have been interpolated from the values at 0.44 and 0.87 μm. The 0.50-μm AERONET channel is not used for interpolation because not all AERONET stations have that channel and the procedure that matches MODIS and AERONET data must be uniform and automatic. Although AERONET does make measurements at 0.675 μm, the values at this wavelength have also been interpolated from 0.44 and 0.87 μm, due to occasional calibration drift at this channel in the AERONET instruments. These calibration issues due to gradual filter degradation are identified and corrected in the quality assured level 2 AERONET data, but unfortunately the collocation with MODIS is done in real-processing time and cannot wait for the postdeployment AERONET calibration corrections. Therefore, the 0.675 μm is not used and, instead, the information is transferred from the more reliable 0.44- and 0.87-μm AERONET channels. Also, the MODIS value at 0.55 μm is not a direct retrieval but an interpolation from the 0.47- and 0.66-μm retrievals; thus, the plot at 0.55 μm in Fig. 8 is a comparison of two interpolated values. The interpolation of AERONET data is done on a log–log plot assuming linearity between 0.44 and 0.87 μm. The error in the interpolation varies between 0% and ~10% depending on the aerosol type (due to nonlinear spectral dependence), with fine-mode-dominated aerosol at high optical thickness introducing the most error, and a mixed- or coarse-dominated aerosol introducing the least (Eck et al. 1999).

Figure 8 represents the scatterplot between MODIS retrievals and AERONET observations, collocated in space and time. The data were sorted according to AERONET aerosol optical thickness. An average was then calculated for every 300 points and plotted. At higher optical thickness where the data become sparser, fewer points are used in the average, as indicated. The standard deviation in each bin is shown by error bars. The regression equation and correlation given at the top of each plot were calculated from the full scatterplots, before binning. The solid black line is the 1:1 line, and the dashed lines denote the expected uncertainty calculated from prelaunch analysis. These dashed lines should encompass one standard deviation (66%) of the aerosol retrievals. The prelaunch expected uncertainty over land is $\Delta\tau = \pm 0.05 \pm 0.15\tau$ (Chu et al. 1998; King et al. 1999). The regression equations in Fig. 8 indicate that MODIS aerosol optical thickness (AOT) offsets at all wavelengths are greater than the expected offset of 0.05 at low optical thickness. Furthermore, these plots show a positive bias at low optical thickness, suggesting a possible instrument calibration issue or, more likely, that surface reflectance may be improperly represented in a systematic way at certain locations and seasons. The regression equations also show that in all wavelengths the slopes are less than one. Ichoku et al. (2003) demonstrate that underprediction of aerosol optical thickness at higher aerosol loadings can be attributed to insufficient light absorption in the aerosol models in certain regions of the world, specifically Africa. This is the reason why the strong absorption model (Table 1) was introduced to the algorithm in the version 4 delivery. The data shown in Fig. 8 and other figures in this paper are combined from *Terra* Collections 003 and 004. We expect the underprediction of optical thickness at high aerosol loading to be less of an issue after reprocessing with the updated algorithm and after performing analyses on only Collection 004 data, but the issue of the offset at low aerosol loading will remain.

Even with the deviations described above, the results of Fig. 8 indicate that the algorithm is retrieving aerosol optical thickness over land to roughly within the expected accuracy. On a global basis, 61%, 68%, and 71% of the retrievals at the 0.47, 0.55, and 0.66 μm, respectively, fall within expected error. From a global perspective, only the blue channel is falling outside of the error bars slightly more often than the prelaunch expectations of 66%. The average τ at 0.55 μm is 0.18 for the land global database at defined AERONET stations. The percent error (relative error) between MODIS retrievals and AERONET observations at 0.55 μm is 41%, showing a positive bias in which MODIS overestimates τ. The overestimate corroborates the positive offsets seen at low to moderate values of optical thickness in Fig. 8. Table 8 shows the percent of retrievals falling within the expected error lines for the entire dataset, as well as grouped by specific region. In some regions the retrievals are poorer than in other regions. Specifically the North American continent, especially Alaska/Canada, is proving to be difficult. This region also exhibits the lowest τ, which contributes to the high relative error. The absolute error in Alaska/Canada is comparable to other regions.

2) VALIDATION OVER OCEAN

Figure 9 represents the scatterplot of 2052 MODIS retrievals over ocean collocated with an AERONET station either on the coast or on an island. Note that the dashed lines, denoting expected uncertainty, are narrower than those over land. The MODIS over-ocean algorithm is expected to be more accurate than the over-land algorithm ($\Delta\tau = \pm 0.03 \pm 0.05\tau$) (Tanré et al. 1999; King et al. 1999). AERONET values at 0.55 and 0.66 μm, are interpolated as in Fig. 8. The MODIS values are not interpolated for these plots. The 0.87-μm plot is the only one showing a directly retrieved

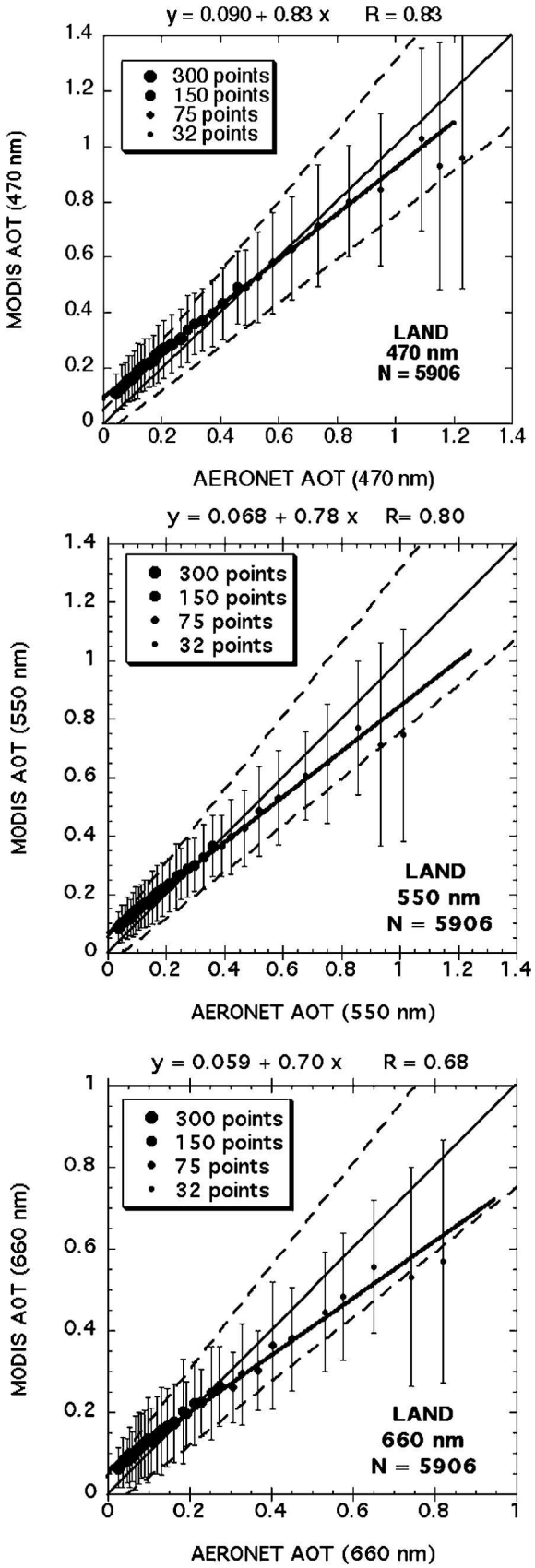

MODIS value plotted against a directly measured AERONET value with no interpolation for either quantity. Unlike the land validation of Fig. 8, the ocean algorithm has virtually no offset and little bias except for a slight underprediction at high optical thickness. The linear regression line follows the 1:1 line closely where most retrievals occur.

Table 8 demonstrates the overall higher accuracy of the ocean retrieval when compared to land in that the percent (relative) error is consistently smaller over ocean than over land. Globally 62%, 66%, and 70% of all retrievals over ocean at 0.55, 0.66, and 0.87 μm, respectively, are falling within the narrowly defined expected uncertainty. Only the 0.55-μm channel is falling outside of the error bars more often than the prelaunch expectations of 66%, albeit slightly. The average τ at 0.55 μm is 0.18 for the ocean global database at defined AERONET stations, the same as for land. Because the land and ocean databases include many of the same stations, this is not surprising. The percent error between MODIS ocean retrievals and AERONET observations at 0.55 μm is only 1%, showing the same absence of bias exhibited in Fig. 9.

Regionally, Table 8 shows that the Asian–Pacific Ocean region and the Saharan–Atlantic Ocean region fall outside the expected uncertainty lines more often than other regions, although for the Sahara it is random scatter with no preference as to over- or underpredicting. The aerosols in these regions can have a strong dust component. Levy et al. (2003) demonstrate that the ocean algorithm does not perform well in a dust-laden atmosphere, attributing the problem to poor assumptions for the dust-aerosol phase functions (i.e., nonsphericity). Empirical nonspherical phase functions have been derived and will be implemented into the next version of the MODIS ocean algorithm. We expect improvements for retrievals in dusty regions to follow from this update.

3) Discussion of validation

Comparison of MODIS retrievals with highly accurate ground-based radiometer data validates the basic retrieval, but does not necessarily validate the product for use in long-term climate studies. Figures 8 and 9 cannot validate the MODIS cloud clearing algorithms

←

FIG. 8. MODIS aerosol optical thickness retrievals over land at 470, 550, and 660 nm as a function of AERONET observations collocated in space and time. The data were sorted according to AERONET aerosol optical thickness and averaged for every 300 points. At higher optical thickness where the data become sparser, fewer points are used in the average, as indicated. The standard deviation in each bin is shown by error bars. The regression equations given at the top of each plot were calculated from the full scatterplots before binning. The dashed lines denote the expected uncertainty calculated from prelaunch analysis.

TABLE 8. Number of retrievals (N), percentage of retrievals (%) falling within expected uncertainty for each wavelength, average optical thickness from AERONET ($\tau^{0.55}$), and percent difference between MODIS and AERONET at 0.55 μm (Diff) for the global dataset and for each region, land, and ocean separately.

Region	N	% 0.47	% 0.55	% 0.66	% 0.87	$\tau_{0.55}$	Diff
All land	5906	61	68	71		0.18	41
China: land	205	71	75	76		0.28	17
India: land	70	70	90	79.		0.46	−2
Mediterranean: land	781	65	67	66		0.20	32
Alaska/Canada: land	178	49	57	67		0.10	122
South Africa: land	347	79	86	84		0.19	−10
South America: land	762	63	72	75		0.18	21
West United States: land	901	56	61	63		0.14	53
East United States: land	1385	55	64	68		0.17	54
East Europe: land	192	79	83	72		0.24	−10
West Europe: land	793	66	72	77		0.17	48
All ocean	2052		62	66	70	0.18	1
Indian Ocean	47		64	77	77	0.16	7
Asian Pacific Ocean	57		56	53	60	0.21	13
Pacific Island ocean	163		70	74	79	0.08	−6
West Mediterranean ocean	334		52	62	68	0.21	−6
East Mediterranean ocean	205		57	63	71	0.23	−7
Saharan ocean	184		58	56	51	0.31	1
Atlantic Isles ocean	146		64	71	71	0.13	8
Australia ocean	70		83	81	83	0.05	2
North Europe ocean	150		65	72	81	0.16	−8
Caribbean ocean	242		62	67	68	0.14	20
East Pacific Ocean	160		52	61	69	0.18	−6
U.S. Atlantic Ocean	288		72	68	70	0.15	7

that play a significant role in the quality of the retrieved aerosol products. Figures 8 and 9 represent the collocated points only for the events in which *both* the MODIS and the AERONET cloud-masking algorithms indicated that no clouds were present. It is possible that MODIS might retrieve, while AERONET identified clouds and did not. Those points would not show up on the scatterplots. If those cases were numerous, long-term MODIS aerosol statistics could be cloud contaminated despite the good agreement in Figs. 8 and 9.

Figures 10a and 10b present an alternative method of validation that checks the long-term statistics for possible cloud contamination. Here we plot monthly mean values in a 3° latitude × 3° longitude box centered on the AERONET station. The data are for the year 2001 at eight selected stations, four with land components and four with only ocean retrievals. Within the four land sites, three of them are near enough to the coast to contain sufficient ocean retrievals within the 3° × 3° box and can be used for testing both land and ocean retrievals. For each location, the monthly mean values of the aerosol optical thickness are plotted in the upper panel, while the difference between the MODIS values and the AERONET values along with prelaunch uncertainty estimates are plotted in the lower panel. Red and blue indicate MODIS retrievals over land and ocean, respectively, while black represents the AERONET observations. The MODIS monthly mean values were calculated from archived MODIS level 3 data (MOD08) on a 1° resolution. Thus, the difficulties with matching MODIS with AERONET in near–real time do not exist, and the monthly AERONET values are calculated from AERONET level 2.0 data. The data from MODIS and AERONET need not be simultaneous. The observations from both instruments were designed to represent monthly mean aerosol optical thickness for each region independently. In this comparison, MODIS does not benefit from AERONET's cloud-clearing algorithm. If MODIS retrievals were systematically cloud contaminated, we would expect the MODIS monthly mean values to be systematically higher than AERONET's. In most cases, MODIS and AERONET exhibit very similar annual cycles, often with very similar magnitudes of optical thickness. Two-thirds of the differences in optical thickness over land are less than 0.10. There is some indication that MODIS retrievals over land may be systematically biased high, but in most cases the difference is still well within the estimated uncertainty of $\pm 0.05 \pm 0.15\tau$. When optical thickness is high and magnitudes significantly differ, as in Cuiaba-Miranda of Fig. 10a, it is AERONET that systematically exceeds MODIS. Over ocean, two-thirds of the differences between MODIS and AERONET monthly means are less than 0.065. The spatial variability across the 3° × 3° box can explain some of these differences, especially at sites like Goddard Space Flight Center (GSFC) and Rome_Tor_Vergata where the ocean retrievals are at least 100 km from the land-based AERONET station. Over the four ocean-only sites the agreement between MODIS and AERONET optical thickness is even better with two-thirds of the monthly means having less than 0.035

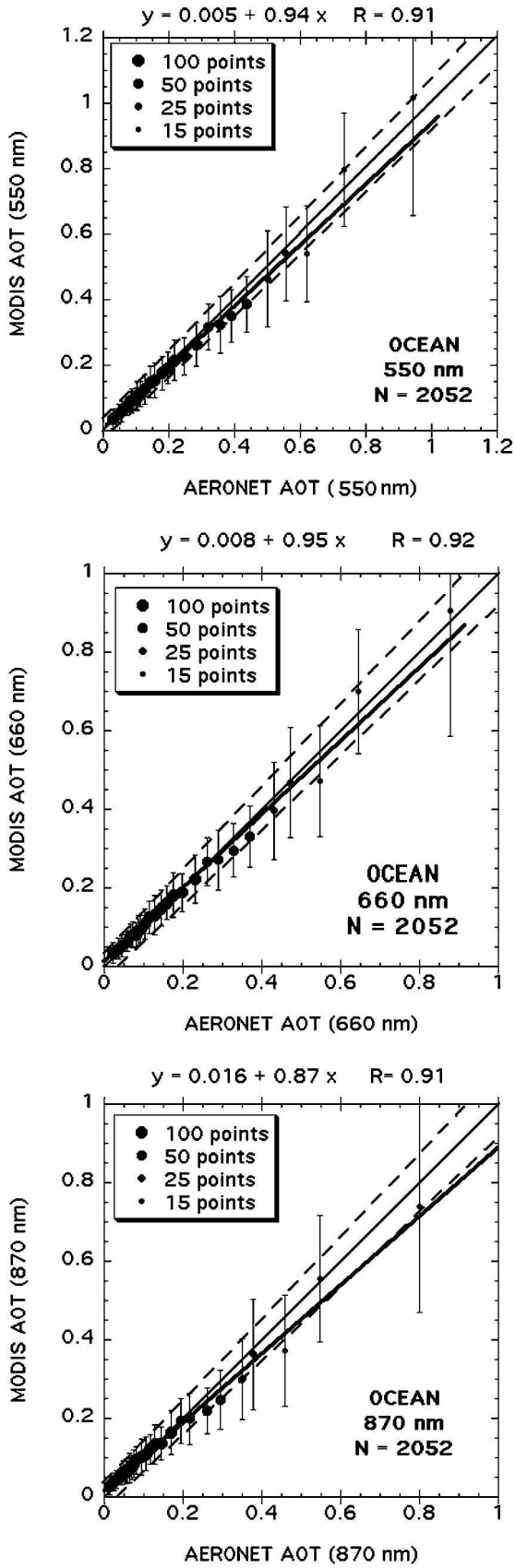

difference in optical thickness. Still, the agreement in optical thickness is striking and suggests that MODIS monthly mean optical thickness values, especially over ocean, are not significantly cloud contaminated and thus can be used with confidence in developing a global aerosol climatology and estimating aerosol forcing.

b. Validation of aerosol size parameters

The validation of retrieved size parameters is not as straightforward as validation of optical thickness. Our primary means of validation is to compare with derivations of the same parameter from inversions of AERONET observed sky radiance (Dubovik et al. 2000). Sky radiance measurements are taken less often than direct sun measurements in the AERONET protocol. Furthermore, sky radiance data must be sufficiently homogenous and the inversion must make a good fit to the measured radiances in order for the retrieval to be used. As a result there are fewer simultaneous data to be plotted in a scatterplot. Because of this we rely primarily on comparisons of monthly means, which test the applicability of the long-term statistics.

Figure 11a and 11b show comparisons of monthly mean MODIS- and AERONET-derived $\eta_{0.55}$ (the ratio of fine mode to total optical thickness). For each location the monthly mean values of the aerosol optical thickness are plotted in the upper panel, while the difference between the MODIS values and the AERONET values along with prelaunch uncertainty estimates for ocean (Tanré et al. 1997) are plotted in the lower panel. Red indicates MODIS retrievals over land, blue over ocean, and black indicates the AERONET observations. The AERONET values are calculated from standard inversions of AERONET observed sky radiance (Dubovik et al. 2000). The MODIS size parameters over land are not expected to be as accurate as the parameters over ocean. Therefore, we focus our discussion on the ocean derivations shown by the blue lines (Tanré et al. 1996). For some sites, such as GSFC, Anmyon, and Male, MODIS-ocean and AERONET agree to within 20% for much of the year. For Bermuda, Midway Island, and Lanai, the agreement is sustained for the first 6 months of the year until the MODIS size parameter drops to a much lower value. These latter ocean stations exhibit very low op-

←

FIG. 9. MODIS aerosol optical thickness retrievals over ocean at 550, 660, and 870 nm as a function of AERONET observations collocated in space and time. The data were sorted according to AERONET aerosol optical thickness and averaged for every 100 points. At higher optical thickness where the data become sparser, fewer points are used in the average, as indicated. The standard deviation in each bin is shown by error bars. The regression equations given at the top of each plot were calculated from the full scatterplots before binning. The dashed lines denote the expected uncertainty calculated from prelaunch analysis.

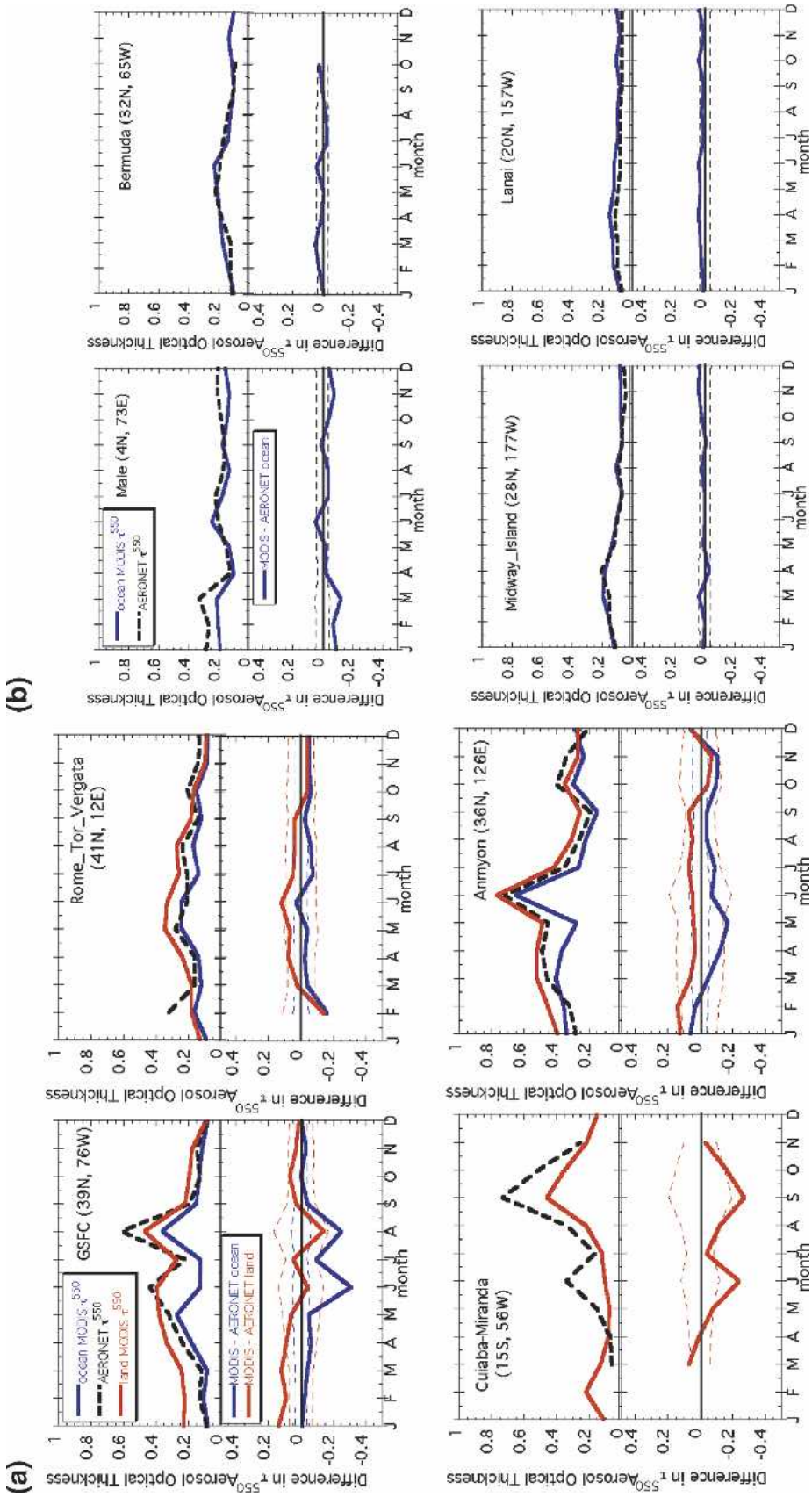

FIG. 10. Monthly mean aerosol optical thickness at 0.55 μm for the year 2001 at (a) four sites with land retrievals and (b) four sites with only ocean retrievals. The top portion of each plot shows the monthly means. The bottom portion shows the difference between MODIS and AERONET values. Also shown by thin dashed lines in the bottom portions are the prelaunch estimated uncertainties of optical thickness retrievals, $\pm 0.03 \pm 0.05\tau$ over ocean and $\pm 0.05 \pm 0.15\tau$ over land. Blue denotes MODIS ocean retrievals, red denotes MODIS land retrievals, and black denotes AERONET. The MODIS values are calculated from level 3 daily statistics and represent a 3° latitude by 3° longitude box centered on the AERONET station.

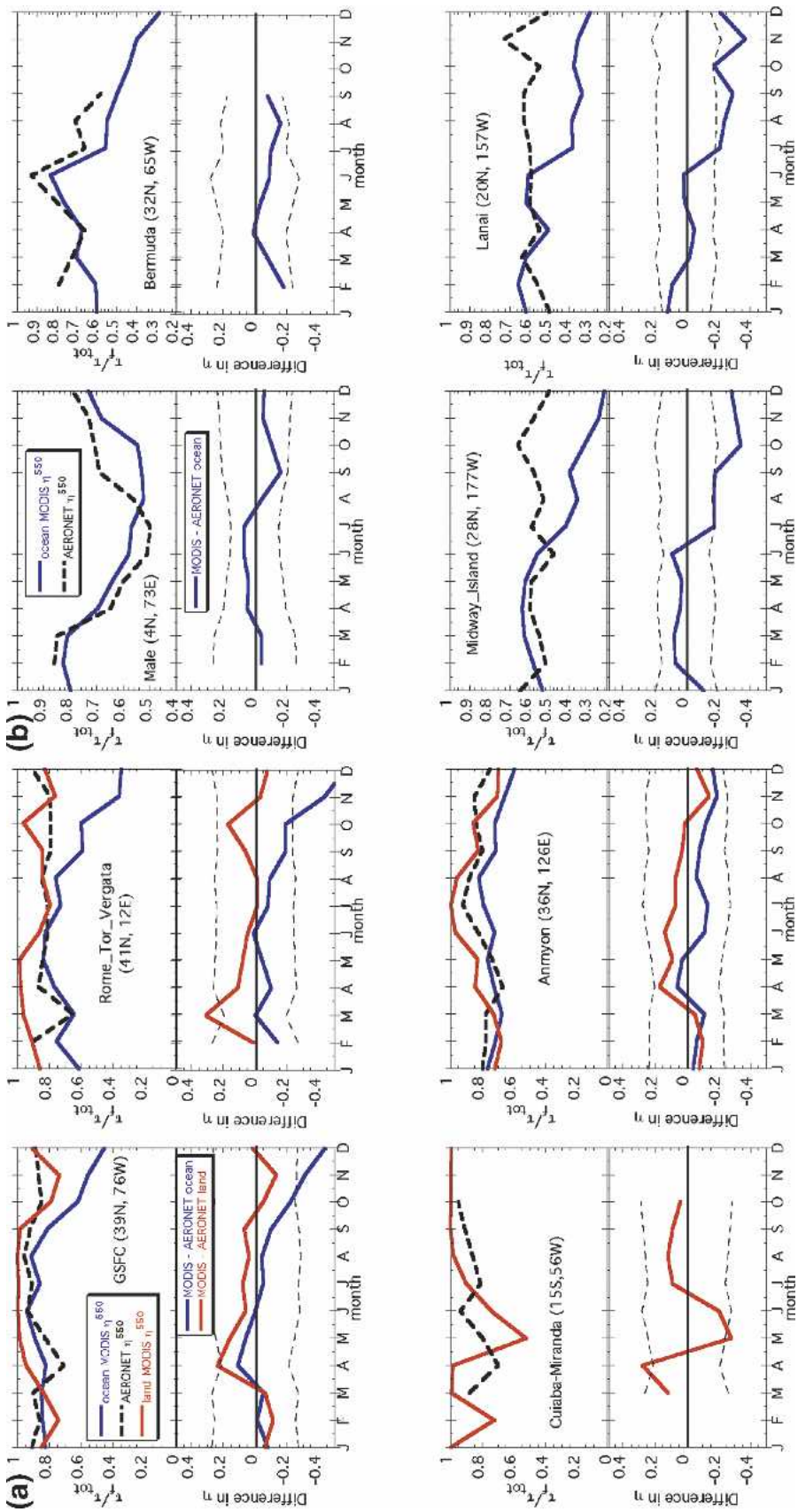

FIG. 11. Monthly mean aerosol fine-mode fraction, η, at 0.55 μm for the year 2001 at (a) four sites with land retrievals and (b) four sites with only ocean retrievals, where η is defined as τ^f/τ^{tot}. The top portion of each plot shows the monthly means. The bottom portion shows the difference between MODIS and AERONET values. Also shown by thin dashed lines in the bottom portions are the prelaunch estimated uncertainties of η retrievals over the ocean, ±30%. Blue denotes MODIS ocean retrievals., red denotes MODIS land retrievals, and black denotes AERONET. The MODIS values are calculated from level 3 daily statistics and represent a 3° latitude × 3° longitude box centered on the AERONET station.

tical thickness. The derivation of size parameters at low optical thickness, when aerosol signal is small, will be very sensitive to instrument calibration. In June 2001, the MODIS instrument suffered an anomaly and the data processing was switched from the B-side to the A-side electronics (http://modis.gsfc.nasa.gov/news/). This switch created a small aberration in the calibration that did not affect the more robust optical thickness retrievals, but did affect the size parameter derivations when optical thickness was low.

Comparison of MODIS-derived particle effective radius and AERONET-derived particle effective radius is shown in Fig. 12. This plot matches MODIS retrievals to daily averages of level 2 quality assured AERONET sky radiance inversions. The MODIS effective radius parameter is for the total bimodal size distribution in which each of the two modes is weighted by η (appendix B). There were 492 MODIS effective radius retrievals collocated with a daily average AERONET retrieval. However, only the 271 matchups with optical thickness greater than 0.15 are plotted in Fig. 12. At low optical thickness, because of less signal, there is greater susceptibility to all algorithmic and sensor uncertainties. These uncertainties include small calibration errors (discussed above) and retrieval errors for both instruments (Ignatov et al. 1998; Remer et al. 2002). These errors make little difference to retrievals of optical thickness but may create large errors in the size parameters. Figure 12 shows that 62% of the points fall within the ± 0.10 μm errors, which is a smaller percentage than what Remer et al. (2002) reported for a more limited dataset. Note that the MODIS and AERONET retrievals both assume spherical particles in deriving size distribution. This assumption causes both MODIS and AERONET to underpredict particle effective radius when nonspherical dust is present (Dubovik et al. 2002b). Thus, the agreement in Fig. 12 may be better at some sites if AERONET retrievals had assumed spheroids instead of spheres (Dubovik et al. 2002b). The MODIS algorithm is being modified to include the option of empirical phase functions that do not require any assumption of particle shape.

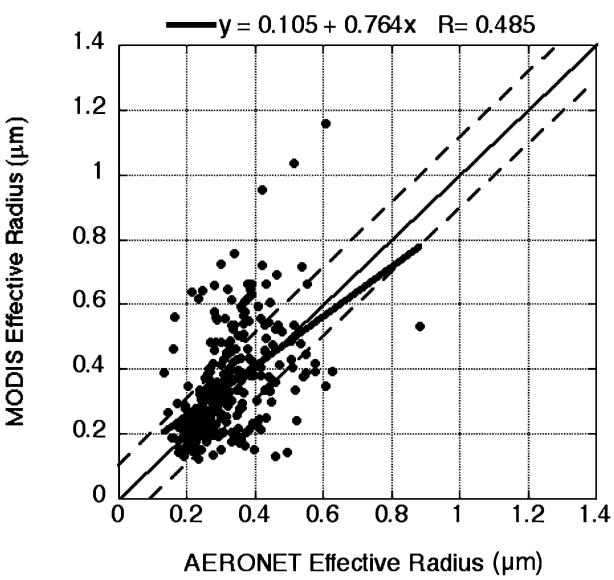

FIG. 12. MODIS-retrieved aerosol particle effective radius over ocean plotted against AERONET retrievals of the same parameter. Only points with AERONET $\tau_{0.44} > 0.15$ are plotted. AERONET values are daily averages for the date of the MODIS overpass. The blue line represents the linear regression through the points, the solid black line is the 1:1 line, and the dashed lines represent ± 0.10 μm; 271 collocated points are shown, and 62% of these points fall within the dashed lines.

5. Results

Figure 13 illustrates the MODIS aerosol retrievals at the global scale. The images are constructed from the aerosol optical thickness and size parameter products both derived from observed MODIS radiances. Red indicates aerosol dominated by small particles (less than 0.5 μm) and greenish tints indicate aerosol with a higher proportion of large particles (greater than 0.5 μm). We can see that aerosol from natural sources, such as sea salt and desert dust, contain larger particles than aerosols emanating from human-produced combustion sources such as agricultural and deforestation burning or urban/industrial pollution. Therefore, aerosol size easily separates aerosols into natural and man-made components [with the exceptions of lightning-initiated forest fire smoke and ocean dimethyl sulfide (DMS) production]. Thus we see that MODIS's ability to separate aerosols by size can be used as a proxy for separating anthropogenic aerosol from natural sources and increases the accuracy of estimating human-induced aerosol forcing (Kaufman et al. 2002).

6. Conclusions

Characterizing the global aerosol system is essential to understanding the earth's climate system and estimating potential global climate change. The MODIS instrument flying aboard NASA's *Terra* and *Aqua* satellites provides a look at the aerosol system over both land and ocean on a daily basis. The derivation of aerosol products from the MODIS-measured radiances relies on the broad spectrum that MODIS measures, ranging from the visible into the mid-infrared, and the 500-m spatial resolution, which allows for better cloud identification and clearing than was possible with previous instruments. The mature MODIS algorithm includes aerosol optical thickness at several wavelengths, information on particle size, and aerosol-reflected flux at the top of the atmosphere, which is expected to be more accurate than the optical thickness retrievals. An

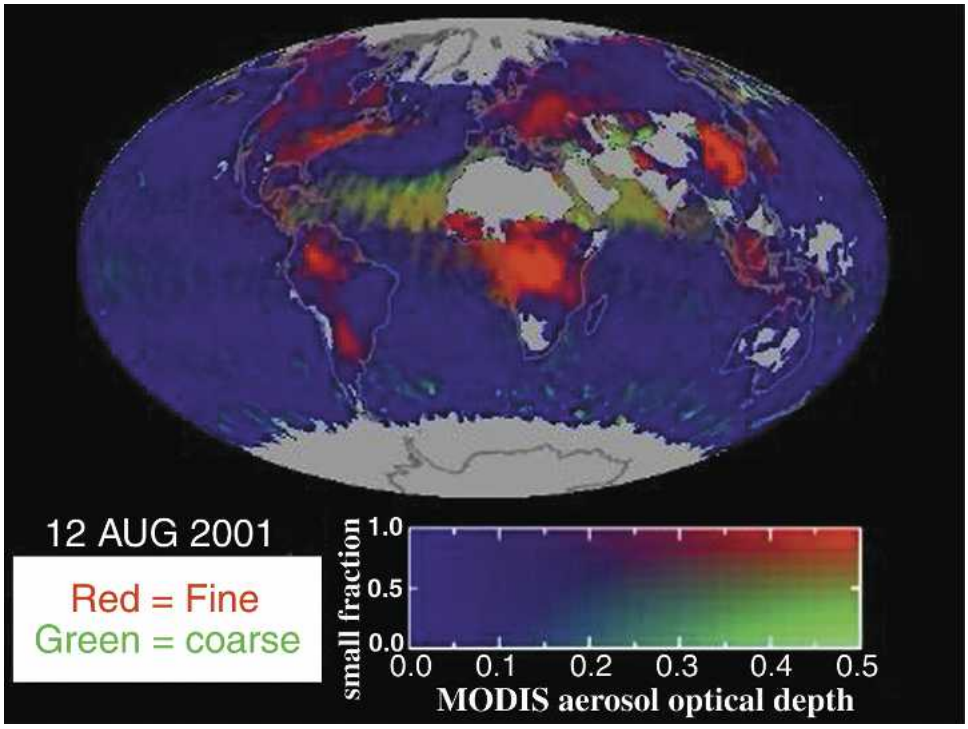

FIG. 13. MODIS aerosol optical thickness at 0.55 μm, representing global aerosol distribution on 12 Aug 2001. The two-dimensional color bar describes both magnitude of optical thickness (along bottom axis) and fraction of optical thickness contributed by smaller fine-mode particles (along vertical axis). Blue indicates low aerosol loading. Red indicates heavy loading of small particles such as pollution and smoke. The greener tones indicate a greater percentage of large particles such as desert dust and sea salt. The image was created from the MODIS daily 10-km resolution data after smoothing the raw data with Gaussian filters applied both in the temporal and spatial domains.

extensive validation effort that collocated over 8000 MODIS retrievals with AERONET measurements of optical thickness show that globally, the MODIS products are accurate to within prelaunch expectations, namely, $\pm 0.05 \pm 0.15\tau$ over land and $\pm 0.03 \pm 0.05\tau$ over ocean. In particular, the retrieval of aerosol over oceans consistently shows remarkably good agreement with virtually no offset or bias through the range of optical thickness where most observations occur. Regional analysis, however, shows specific issues for certain locations. Comparison of MODIS and AERONET monthly means at eight specific locations scattered globally demonstrates that the MODIS retrievals are not affected by cloud contamination at those sites, and that MODIS long-term statistics agree with AERONET to within 0.10 over land and to within 0.035 at oceanic island sites. MODIS-derived aerosol size parameters are in general agreement with the same quantities derived by AERONET instruments on the ground. For moderate optical thickness, one standard deviation of MODIS effective radius retrievals falls within ± 0.11 μm of AERONET measurements. Comparison of MODIS and AERONET monthly mean values of η, the ratio of fine-mode aerosol optical thickness to total optical thickness at eight specific sites suggests that over-ocean MODIS values agree to within 20%, which exceeds the prelaunch estimate of $\pm 30\%$ for individual retrievals. However, at low aerosol optical thickness ($\tau < 0.15$) the MODIS size retrievals are susceptible to small aberrations in the calibration and other factors, which introduce greater uncertainty. In addition, dust, with its nonspherical shapes, introduce uncertainty in both the optical thickness and size parameter retrievals. This latter issue will be addressed with the incorporation of nonspherical phase functions into the next version of the algorithms. In the meantime, the MODIS aerosol products are sufficiently accurate for a variety of applications, including improved estimates of observationally based aerosol radiative effects.

Acknowledgments. We thank the many AERONET principal investigators and site managers who provided the data used in the validation analysis. In particular we acknowledge the contribution of Charles McClain and the SIMBIOS project, which maintains many of the AERONET sites used in the over-ocean validation. The MODIS aerosol product is the culmination of effort by many diverse people and groups including Vincent Salomonson, MODIS team leader, Michael King, EOS senior project scientist, Ed Masuoka and Richard

Hucek of the MODIS Science Data Support Team (SDST), the MODIS Characterization Support Team (MCST), and the Goddard Distributed Active Archive Center (GDAAC). NASA's Earth Science Enterprise has provided continuous funding that has supported the decade-long effort of deriving, implementing, and validating the algorithms. We also acknowledge the contribution of the many users of the MODIS aerosol product whose numerous questions prompted us to compile the answers to their questions into this paper, and last, we thank Jonathan Harris who proofread the manuscript.

APPENDIX A

Fraction of Fine-Mode Optical Thickness

One of the most important products produced by the algorithm is the ratio of fine-mode optical thickness to the total optical thickness, or simply the fraction of fine mode. Here we show that this fraction at 0.55 μm is the same parameter as η, the reflectance weighting parameter. We start with Eq. (6),

$$\rho_\lambda^{\mathrm{LUT}}(\tau_{0.55}^{\mathrm{tot}}) = \eta\rho_\lambda^{\mathrm{f}}(\tau_{0.55}^{\mathrm{tot}}) + (1-\eta)\rho_\lambda^{\mathrm{c}}(\tau_{0.55}^{\mathrm{tot}}), \quad \text{(A1)}$$

where $\rho_\lambda^{\mathrm{f}}$ and $\rho_\lambda^{\mathrm{c}}$ are the fine- and coarse-mode atmospheric reflectances for the same optical thickness as the total spectral reflectance, $\rho_\lambda^{\mathrm{LUT}}$, respectively, and η is the reflectance weighting parameter. Note that $\rho^{\mathrm{LUT}}\lambda \neq \rho^{\mathrm{f}}\lambda + \rho^{\mathrm{c}}\lambda$, and that the total and component reflectances all are functions of the total optical thickness ($\tau_{0.55}^{\mathrm{tot}}$), not the component optical thicknesses ($\tau_{0.55}^{\mathrm{f}}$ and $\tau_{0.55}^{\mathrm{c}}$). All optical thicknesses are defined at 0.55 μm. This is by definition in constructing the lookup tables.

Define the total optical thickness ($\tau_{0.55}^{\mathrm{tot}}$) equal to the sum of the fine ($\tau_{0.55}^{\mathrm{f}}$) and coarse ($\tau_{0.55}^{\mathrm{c}}$) components. Using the single scattering approximation,

$$\rho_\lambda^{\mathrm{f}} = C\tau_{0.55}^{\mathrm{tot}}P_\lambda^{\mathrm{f}},\ \rho_\lambda^{\mathrm{c}} = C\tau_{0.55}^{\mathrm{tot}}P_\lambda^{\mathrm{c}} \quad \text{(A2)}$$

and

$$\rho_\lambda^{\mathrm{LUT}} = C(\tau_{0.55}^{\mathrm{f}}P_\lambda^{\mathrm{f}} + \tau_{0.55}^{\mathrm{c}}P_\lambda^{\mathrm{c}}), \quad \text{(A3)}$$

where C is a constant depending on geometry, and P_λ^{f} and P_λ^{c} are the fine-mode and coarse-mode phase functions calculated for the lookup tables, respectively. There is no P_λ^{tot} because the phase functions in the lookup table are calculated for the collection of individual fine and coarse modes, not for any "total" aerosol size distribution. Solving for η in Eq. (A1) gives

$$\eta = (\rho_\lambda^{\mathrm{LUT}} - \rho_\lambda^{\mathrm{c}})/(\rho_\lambda^{\mathrm{f}} - \rho_\lambda^{\mathrm{c}}). \quad \text{(A4)}$$

Substituting (A2) and (A3) into (A4) gives

$$\eta = [C(\tau_{0.55}^{\mathrm{f}}P_\lambda^{\mathrm{f}} + \tau_{0.55}^{\mathrm{c}}P_\lambda^{\mathrm{c}}) - C\tau_{0.55}^{\mathrm{tot}}P_\lambda^{\mathrm{c}}]/(C\tau_{0.55}^{\mathrm{tot}}P_\lambda^{\mathrm{f}} - C\tau_{0.55}^{\mathrm{tot}}P_\lambda^{\mathrm{c}}). \quad \text{(A5)}$$

Dropping the constant C and using the definition of $\tau_{0.55}^{\mathrm{tot}} = \tau_{0.55}^{\mathrm{f}} + \tau_{0.55}^{\mathrm{c}}$ gives

$$\eta = (\tau_{0.55}^{\mathrm{f}}P_\lambda^{\mathrm{f}} + \tau_{0.55}^{\mathrm{c}}P_\lambda^{\mathrm{c}}) - \tau_{0.55}^{\mathrm{f}}P_\lambda^{\mathrm{c}} - \tau_{0.55}^{\mathrm{c}}P_\lambda^{\mathrm{c}})/[\tau_{0.55}^{\mathrm{tot}}(P^{\mathrm{f}}\lambda - P_\lambda^{\mathrm{c}})], \quad \text{(A6)}$$

$$\eta = \tau_{0.55}^{\mathrm{f}}(P_\lambda^{\mathrm{f}} - P_\lambda^{\mathrm{c}})/[\tau_{0.55}^{\mathrm{tot}}(P_\lambda^{\mathrm{f}} - P_\lambda^{\mathrm{c}})], \quad \text{(A7)}$$

$$\eta = \tau_{0.55}^{\mathrm{f}}/\tau_{0.55}^{\mathrm{tot}}. \quad \text{(A8)}$$

Thus the reflectance weighting factor, η, is also the ratio between fine mode and total optical thickness at 0.55 μm, as defined within the parameters of the inversion.

APPENDIX B

Definitions of Derived Parameters

The following give the formulas for derivation of the derived parameters. In these formulas $n(r)$ is the size distribution with r denoting radius, r_g the geometric mean radius, and N_{o} the number of particles per cross section of the atmospheric column (the amplitude of a lognormal number size distribution) that can be converted from V_{o} of the volume size distributions for each lognormal mode using

$$N_{\mathrm{O}} = \frac{3\sigma V_{\mathrm{O}}\sqrt{2\pi}}{4\pi} r_g^{-3} \exp\left(-\frac{9}{2}\sigma^2\right).$$

The scattering coefficient β_s is specific to each model mode, ρ is the density of the particle assumed to be 1 g cm^{-3}, erf( ) is the error function, σ is ln σ_g where σ_g is the geometric mean standard deviation of the lognormal distribution, μ is cos θ, where θ is the scattering angle, P( ) is the phase function, τ is the optical thickness and, unless designated specifically for wavelength or large or small mode, represents the total optical thickness at 0.55 μm. Extcoeff is the extinction coefficient, and unless designated specifically for wavelength is understood to be 0.55 μm. Cloud condensation nuclei in units of cm^{-2} is:

$$\mathrm{CCN} = \int_{r_{\mathrm{O}}=0.03\mu\mathrm{m}}^{\infty} n(r)dr = 0.5\times10^{-10}\left(1 - \mathrm{erf}\left\{\frac{\ln(r_{\mathrm{o}}/r_{\mathrm{g}})}{\sqrt{2}\sigma}\right\}\right).$$

Asymmetry factor:

$$g_\lambda = 0.5\int_{-1}^{1}\mu P\lambda(\mu)d\mu = 0.5\int_0^{\pi}\cos(\theta)P\lambda(\theta)\sin\theta d\theta.$$

Backscattering ratio:

$$\beta_\lambda = \frac{1}{2\pi}\int_{-1}^{1}\frac{1}{\mu}P(\mu)\mathrm{d}\mu = \frac{1}{2\pi}\int_0^{\pi}\theta P(\theta)\sin\theta d\theta.$$

Number of particles in each mode (1 cm^{-3}), and τ and extcoeff defined at 0.55 μm:

$$N_{\text{small}} = \frac{\tau_{\text{small}}}{\text{extcoeff}_{\text{small}}} \qquad N_{\text{large}} = \frac{\tau_{\text{large}}}{\text{extcoeff}_{\text{large}}},$$

Moments of M^k of order k:

$$M^k = \int_{\text{o}}^{\infty} r^k n(r) dr = (r_g)^k \exp(0.5k^2\sigma^2).$$

Effective radius (μm):

$$r_{\text{eff}} = (N_{\text{small}}M^3_{\text{small}} + N_{\text{large}}M^3_{\text{large}})/(N_{\text{small}}M^2_{\text{small}} + N_{\text{large}}M^2_{\text{large}}).$$

Mass concentration (μg per cm^2),

$$\text{Mass_conc} = N_{\text{small}}M^3_{\text{small}} + N_{\text{large}}M^3_{\text{large}}, \quad \text{over ocean}$$

$$\text{Mass_conc} = \frac{4\pi\rho}{3}\left\{\eta\left(\frac{N_o r_g^3 \tau_{0.66}}{\beta_S}\right)_{\text{small}} + (1-\eta)\left(\frac{N_o r_g^3 \tau_{0.66}}{\beta_S}\right)_{\text{large}}\right\}, \quad \text{over land}$$

Ångström exponent 1 (0.55/0.87) and Ångström exponent 2 (0.87/2.13):

$$\text{AngExp_1} = \frac{\ln\left(\frac{\tau_{0.55}}{\tau_{0.87}}\right)}{\ln\left(\frac{0.55}{0.87}\right)}$$

$$\text{AngExp_2} = \frac{\ln\left(\frac{\tau_{0.87}}{\tau_{2.13}}\right)}{\ln\left(\frac{0.87}{2.13}\right)}.$$

APPENDIX C

Recommendations for Using Products

There are many choices for aerosol optical thickness. The products in Tables 4–7 labeled as validated, not yet validated, or derived are recommended. Corrected_Optical_Depth_Land is the recommended spectral product over land, and Effective_Optical_Depth_Average_Ocean is the recommended spectral product over ocean. Products such as Continental_Optical_Depth_Land are intermediate parameters and should be used only as a diagnostic.

The word "small" in the product name indicates fine mode so that Optical_Depth_Small is the fine-mode optical thickness, τ^f, from appendix A. Optical_Depth_Ratio_Small is the fine-mode ratio, η_λ. Likewise, the word "large" indicates coarse mode. The word "average" indicates the solution averaged from all retrieval solutions with fitting error less than 3% or the average of the three best solutions if all $\varepsilon > 3\%$. The word "best" indicates the single solution with the least error, ε, no matter how large. See Eq. (7). The recommendation is to use those products labeled as average.

The Ångström exponent over land is defined for wavelengths 0.47 and 0.66 μm. There are two Ångström exponents for the ocean parameters, one defined using wavelengths 0.55 and 0.87 μm and the other using 0.87 and 2.13 μm.

Aerosol_Type under the land products is a function mostly of geography and season and should not be considered a retrieved quantity. The Cloud_Fraction listed in the tables is not a true cloud fraction, but instead an indication of the fraction of pixels not used in the retrieval due to a combination of clouds, surface issues, or internal inconsistencies. Likewise, Mean_Reflectance is the mean reflectance only of those pixels that survive the masking and elimination procedures and are actually used in the retrievals. Solution_Index tells which fine and coarse aerosol models were chosen in the retrieval. Least_Squares_Error reports the fitting error of the inversion, ε, from Eq. (7).

The Quality_Assurance parameters are five-byte codes that hold information concerning the retrievals and the overall quality. Details of the Quality_Assurance code are given by the MODIS Atmosphere's Quality Assurance Plan, which can be found online at http://modis-atmos.gsfc.nasa.gov.

REFERENCES

Ackerman, S. A., K. I. Strabala, W. P. Menzel, R. A. Frey, C. C. Moeller, and L. E. Gumley, 1998: Discriminating clear sky from clouds with MODIS. *J. Geophys. Res.,* **103,** 32 139–32 140.

Ahmad, Z., and R. S. Fraser, 1982: An iterative radiative transfer code for the ocean–atmosphere system. *J. Atmos. Sci.,* **39,** 656–665.

Chu, D. A., Y. J. Kaufman, L. A. Remer, and B. N. Holben, 1998: Remote sensing of smoke from MODIS airborne simulator during the SCAR-B experiment. *J. Geophys. Res.,* **103,** 31 979–31 988.

——, ——, C. Ichoku, L. A. Remer, D. Tanre, and B. N. Holben, 2002: Validation of MODIS aerosol optical depth retrieval over land. *Geophys. Res. Lett.,* **29,** 8007, doi:10.1029/2001GL013205.

Dubovik, O., A. Smirnov, B. N. Holben, M. D. King, Y. J. Kaufman, T. F. Eck, and I. Slutsker, 2000: Accuracy assessments of aerosol optical properties retrieved from AERONET sun and sky-radiance measurements. *J. Geophys. Res.,* **105,** 9791–9806.

——, B. N. Holben, T. F. Eck, A. Smirnov, Y. J. Kaufman, M. D. King, D. Tanré, and I. Slutsker, 2002a: Variability of absorption and optical properties of key aerosol types observed in worldwide locations. *J. Atmos. Sci.,* **59,** 590–608.

——, ——, T. Lapyonok, A. Sinyk, M. I. Mishchenko, P. Yang, and I. Slutsker, 2002b: Non-spherical aerosol retrieval method employing light scattering by spheroids. *Geophys. Res. Lett.,* **29,** 1415, doi:10.1029/2001GL014506.

Eck, T. F., B. N. Holben, J. S. Reid, O. Dubovik, A. Smirnov, N. T. O'Neill, I. Slutsker, and S. Kinne, 1999: Wavelength dependence of the optical depth of biomass burning, urban and desert dust aerosols. *J. Geophys. Res.,* **104,** 31 333–31 349.

——, and Coauthors, 2003: Variability of biomass burning aerosol optical characteristics in southern Africa during the SAFARI 2000 dry season campaign and a comparison of single scattering albedo estimates from radiometric measurements. *J. Geophys. Res.,* **108,** 8477, doi:10.1029/2002JD002321.

Gao, B.-C., Y. J. Kaufman, D. Tanré, and R.-R. Li, 2002: Distin-

guishing tropospheric aerosols from thin cirrus clouds for improved aerosol retrievals using the ratio of 1.38-μm and 1.24-μm channels. *Geophys. Res. Lett.,* **29,** 1890, doi:10.1029/2002GL015475.

Guenther, B., X. Xiong, V. V. Salomonson, W. L. Barnes, and J. Young, 2002: On-orbit performance of the Earth Observing System Moderate Resolution Imaging Spectroradiometer: First year of data. *Remote Sens. Environ.,* **83,** 16–30.

Herman, J. R., P. K. Bhartia, O. Torres, C. Hsu, C. Seftor, and E. Celarier, 1997: Global distribution of UV-absorbing aerosols from Nimbus 7/TOMS data. *J. Geophys. Res.,* **102,** 16 911–16 922.

Holben, B. N., and Coauthors, 1998: AERONET—A federated instrument network and data archive for aerosol characterization. *Remote Sens. Environ.,* **66,** 1–16.

Houghton, J. T., Y. Ding, D. J. Griggs, M. Noguer, P. J. van der Linden, and D. Xiaosu, Eds., 2001: *Climate Change 2001: The Scientific Basis.* Cambridge University Press, 944 pp.

Husar, R. B., L. L. Stowe, and J. M. Prospero, 1997: Characterization of tropospheric aerosols over the oceans with the NOAA Advanced Very High Resolution Radiometer optical thickness operational product. *J. Geophys. Res.,* **102,** 16 889–16 910.

Ichoku, C., D. A. Chu, S. Mattoo, Y. J. Kaufman, L. A. Remer, D. Tanré, I. Slutsker, and B. N. Holben, 2002: A spatio-temporal approach for global validation and analysis of MODIS aerosol products. *Geophys. Res. Lett.,* **29,** doi:10.1029/2001GL013206.

——, L. A. Remer, Y. J. Kaufman, R. Levy, D. A. Chu, D. Tanré, and B. N. Holben, 2003: MODIS observation of aerosols and estimation of aerosol radiative forcing over southern Africa during SAFARI 2000. *J. Geophys. Res.,* **108,** 8006, doi:10.1029/2002JD002366.

——, ——, and T. F. Eck, 2005: Quantitative evaluation and intercomparison of morning and afternoon MODIS aerosol measurements from the Terra and Aqua satellites. *J. Geophys. Res.,* in press.

Ignatov, A., L. Stowe, and R. Singh, 1998: Sensitivity study of the Angstrom exponent derived from AVHRR over oceans. *Adv. Space Res.,* **21,** 439–442.

——, and Coauthors, 2005: Two MODIS aerosol products over ocean on the *Terra* and *Aqua* CERES SSF datasets. *J. Atmos. Sci.,* **62,** 1008–1031.

Kaufman, Y. J., 1989: The atmospheric effect on remote sensing and its correction. *Theory and Applications of Optical Remote Sensing,* G. Asrar, Ed., John Wiley & Sons, 336–428.

——, D. Tanré, L. A. Remer, E. Vermote, A. Chu, and B. N. Holben, 1997a: Operational remote sensing of tropospheric aerosol over land from EOS Moderate Resolution Imaging Spectroradiometer. *J. Geophys. Res.,* **102,** 17 051–17 067.

——, A. E. Wald, L. A. Remer, B.-C. Gao, R.-R. Li, and L. Flynn, 1997b: The MODIS 2.1 μm Channel—Correlation with visible reflectance for use in remote sensing of aerosol. *IEEE Trans. Geosci. Remote Sens.,* **35,** 1286–1298.

——, D. Tanré, and O. Boucher, 2002: A satellite view of aerosols in the climate system. *Nature,* **419,** 215–223.

King, M. D., Y. J. Kaufman, D. Tanré, and T. Nakajima, 1999: Remote sensing of tropospheric aerosols from space: Past, present, and future. *Bull. Amer. Meteor. Soc.,* **80,** 2229–2259.

——, and Coauthors, 2003: Cloud and aerosol properties, precipitable water, and profiles of temperature and humidity from MODIS. *IEEE Trans. Geosci. Remote Sens.,* **41,** 442–458.

Levy, R. C., and Coauthors, 2003: Evaluation of the MODIS retrievals of dust aerosol over the ocean during PRIDE. *J. Geophys. Res.,* **108**, 8594, doi:10.1029/2002JD002460.

——, L. A. Remer, J. V. Martins, Y. J. Kaufman, A. Plana-Fattori, J. Redemann, P. B. Russell, and B. Wenny, 2005: Evaluation of the MODIS aerosol retrievals over ocean and land during CLAMS. *J. Atmos. Sci.,* **62,** 974–992.

Li, R.-R., Y. J. Kaufman, B.-C. Gao, and C. O. Davis, 2003: Remote sensing of suspended sediments and shallow coastal waters. *IEEE Trans. Geosci. Remote Sens.,* **41,** 559–566.

Martins, J. V., D. Tanré, L. A. Remer, Y. J. Kaufman, S. Mattoo, and R. Levy, 2002: MODIS cloud screening for remote sensing of aerosol over oceans using spatial variability. *Geophys. Res. Lett.,* **29,** 8009, doi:10.1029/2001GL013252.

MCST, 2000: MODIS level 1B product user's guide, for level 1B version 2.3.x, release 2. MCST Document PUB-01-U-DNCN, 47 pp. [Available online at http://www.mcst.ssai.biz/mcstweb/L1B/product.html.]

——, 2002: MODIS level 1B product user's guide, for level 1B version 4.0.9 (Terra) and version 4.1.1 (Aqua). MCST Document PUB-01-U-0202-REV B, MCST Internal Memo, M1039, 61 pp. [Available online at http://www.mcst.ssai.biz/mcstweb/L1B/product.html.]

Prins, E. M., J. M. Feltz, W. P. Menzel, and D. E. Ward, 1998: An overview of GOES-8 diurnal fire and smoke results for SCAR-B and 1995 fire season in South America. *J. Geophys. Res.,* **103,** 31 821–31 836.

Remer, L. A., and Y. J. Kaufman, 1998: Dynamical aerosol model: Urban/industrial aerosol. *J. Geophys. Res.,* **103,** 13 859–13 871.

——, ——, B. N. Holben, A. M. Thompson, and D. McNamara, 1998: A model of tropical biomass burning smoke aerosol size distribution. *J. Geophys. Res.,* **103,** 31 879–31 892.

——, and Coauthors, 2002: Validation of MODIS aerosol retrieval over ocean. *Geophys. Res. Lett.,* **29,** 8008, doi:10.1029/2001GL013204.

Rosenfield, D., and I. M. Lensky, 1998: Satellite-based insights into precipitation formation processes in continental and maritime convective clouds. *Bull. Amer. Meteor. Soc.,* **79,** 2457–2476.

Samet, J. M., S. L. Zeger, F. Dominici, F. Curriero, I. Coursac, D. W. Dockery, J. Schwartz, and A. Zanobetti, 2000: The national morbidity, mortality, and air pollution study, Part II: Morbidity, mortality, and air pollution in the United States. Health Effects Institute Research Rep. 94, Cambridge, MA, 87 pp.

Smirnov, A., B. N. Holben, T. F. Eck, O. Dubovik, and I. Slutsker, 2000: Cloud-screening and quality control algorithms for the AERONET database. *Remote Sens. Environ.,* **73,** 337–349.

Swap, R. J., H. J. Annegarn, J. T. Suttles, M. D. King, S. Platnick, J. L. Privette, and R. J. Scholes, 2003: Africa burning: A thematic analysis of the Southern African Regional Science Initiative (SAFARI 2000). *J. Geophys. Res.,* **108,** 8465, doi:10.1029/2003JD003747.

Tanré, D., M. Herman, and Y. J. Kaufman, 1996: Information on aerosol size distribution contained in solar reflected spectral radiances. *J. Geophys. Res.,* **101,** 19 043–19 060.

——, Y. J. Kaufman, M. Herman, and S. Mattoo, 1997: Remote sensing of aerosol properties over oceans using the MODIS/EOS spectral radiances. *J. Geophys. Res.,* **102,** 16 971–16 988.

——, L. A. Remer, Y. J. Kaufman, S. Mattoo, P. V. Hobbs, J. M. Livingston, P. B. Russell, and A. Smirnov, 1999: Retrieval of aerosol optical thickness and size distribution over ocean from the MODIS Airborne Simulator during TARFOX. *J. Geophys. Res.,* **104,** 2261–2278.

Torres, O., P. K. Bhartia, J. R. Herman, A. Sinyuk, P. Ginoux, and B. Holben, 2002: A long-term record of aerosol optical depth from TOMS observations and comparison to AERONET measurements. *J. Atmos. Sci.,* **59,** 398–413.

Twomey, S. A., 1977: The influence of pollution on the shortwave albedo of clouds. *J. Atmos. Sci.,* **34,** 1149–1152.